



HAL
open science

Gut microbiota remodeling and intestinal adaptation to lipid malabsorption after enteroendocrine cell loss in adult mice

Florence Blot, Justine Marchix, Miriam Ejarque, Sara Jimenez, Aline Meunier, Céline Keime, Camille Trottier, Mikaël Croyal, Céline Lapp, Maxime Mahe, et al.

► To cite this version:

Florence Blot, Justine Marchix, Miriam Ejarque, Sara Jimenez, Aline Meunier, et al.. Gut microbiota remodeling and intestinal adaptation to lipid malabsorption after enteroendocrine cell loss in adult mice. Cellular and Molecular Gastroenterology and Hepatology, 2023, 10.1016/j.jcmgh.2023.02.013 . hal-04007457

HAL Id: hal-04007457

<https://hal.science/hal-04007457>

Submitted on 12 Oct 2023

HAL is a multi-disciplinary open access archive for the deposit and dissemination of scientific research documents, whether they are published or not. The documents may come from teaching and research institutions in France or abroad, or from public or private research centers.

L'archive ouverte pluridisciplinaire **HAL**, est destinée au dépôt et à la diffusion de documents scientifiques de niveau recherche, publiés ou non, émanant des établissements d'enseignement et de recherche français ou étrangers, des laboratoires publics ou privés.

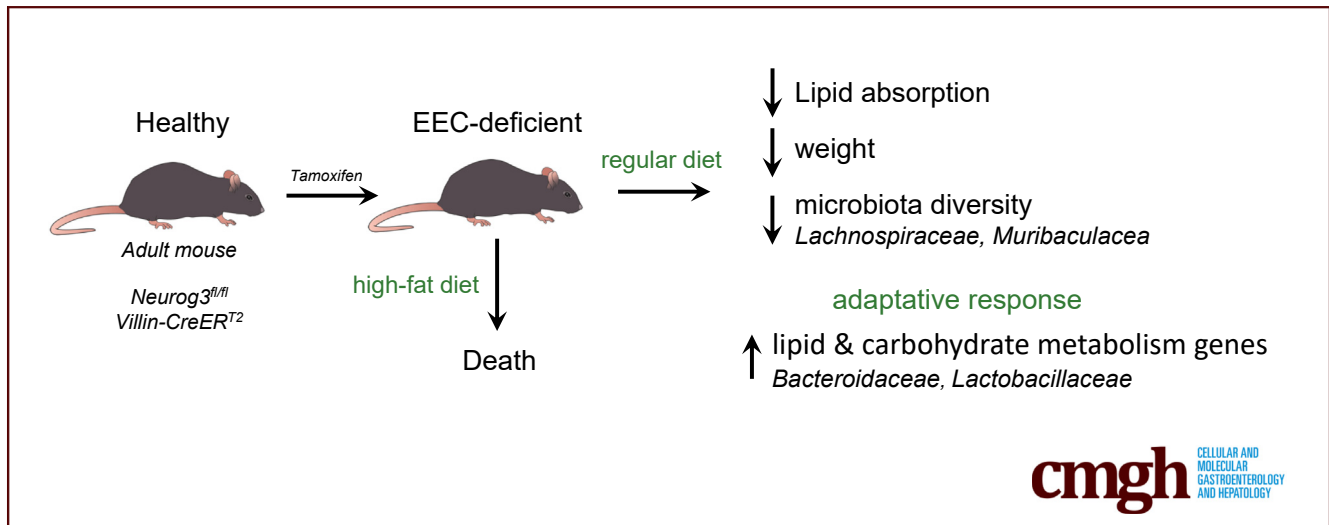
ORIGINAL RESEARCH

Gut Microbiota Remodeling and Intestinal Adaptation to Lipid Malabsorption After Enteroendocrine Cell Loss in Adult Mice



Florence Blot,^{1,2,3,4} Justine Marchix,⁵ Miriam Ejarque,^{1,2,3,4} Sara Jimenez,^{1,2,3,4} Aline Meunier,^{1,2,3,4} Céline Keime,^{1,2,3,4} Camille Trottier,⁵ Mikael Croyal,^{6,7,8} Céline Lapp,^{1,2,3,4} Maxime M. Mahe,^{5,9,10} Adèle De Arcangelis,^{1,2,3,4} and Gérard Gradwohl^{1,2,3,4}

¹Institut de Génétique et de Biologie Moléculaire et Cellulaire (IGBMC), Illkirch, France; ²Institut National de la Santé et de la Recherche Médicale (INSERM) U1258, Illkirch, France; ³Centre National de Recherche Scientifique (CNRS) UMR7104, Illkirch, France; ⁴Université de Strasbourg, Illkirch, France; ⁵Nantes Université, CHU Nantes, Inserm, TENS, The Enteric Nervous System in Gut and Brain Diseases, IMAD, Nantes, France; ⁶L'Institut du Thorax, INSERM UMR_S1087, CNRS UMR_6291, Université de Nantes, Nantes, France; ⁷CRNH-Ouest Mass Spectrometry Core Facility, Nantes, France; ⁸Nantes Université, CHU Nantes, Inserm, CNRS, SFR Santé, Inserm UMS 016, CNRS UMS 3556, Nantes, France; ⁹Department of Pediatric General and Thoracic Surgery, Cincinnati Children's Hospital Medical Center, Cincinnati, Ohio; and ¹⁰Department of Pediatrics, University of Cincinnati, Cincinnati, Ohio



SUMMARY

Enteroendocrine cell depletion in healthy adult male mice leads to rapid gut microbiota remodeling. Intestinal lipid absorption is impaired and spatially delayed. Transcriptional changes suggest adaptation mechanisms to remedy decreased food efficacy and adjust energy utilization.

BACKGROUND & AIMS: Enteroendocrine cells (EECs) and their hormones are essential regulators of whole-body energy homeostasis. EECs sense luminal nutrients and microbial metabolites and subsequently secrete various hormones acting locally or at a distance. Impaired development of EECs during embryogenesis is life-threatening in newborn mice and humans due to compromised nutrient absorption. However, the physiological importance of the EEC system in adult mice has yet to be directly studied. Herein, we aimed to determine the long-term consequences of a total loss of EECs in healthy adults on energy metabolism, intestinal transcriptome, and microbiota.

METHODS: We depleted intestinal EECs by tamoxifen treatment of adult *Neurog3^{fl/fl}; Villin-CreER^{T2}* male mice. We studied intestinal cell differentiation, food efficiency, lipid absorption, microbiota composition, fecal metabolites, and transcriptomic responses in the proximal and distal small intestines of mice lacking EECs. We also determined the high-fat diet-induced transcriptomic changes in sorted *Neurog3^{eYFP/+}* EECs.

RESULTS: Induction of EEC deficiency in adults is not life-threatening unless fed with a high-fat diet. Under a standard chow diet, mice lose 10% of weight due to impaired food efficiency. Blood concentrations of cholesterol, triglycerides, and free fatty acids are reduced, and lipid absorption is impaired and delayed in the distal small intestine. Genes controlling lipogenesis, carbohydrate metabolism, and neoglucogenesis are upregulated. Microbiota composition is rapidly altered after EECs depletion and is characterized by decreased α -diversity. *Bacteroides* and *Lactobacillus* were progressively enriched, whereas *Lachnospiraceae* declined without impacting fecal short-chain fatty acid concentrations.

CONCLUSIONS: EECs are dispensable for survival in adult male mice under a standard chow diet. The absence of EECs impairs intestinal lipid absorption, leading to transcriptomic and metabolic adaptations and remodeling of the gut microbiota. (*Cell Mol Gastroenterol Hepatol* 2023;15:1443–1461; <https://doi.org/10.1016/j.jcmgh.2023.02.013>)

Keywords: Enteroendocrine Cells; Food Efficiency; Lipid Absorption; Microbiota.

See editorial on page 1535.

Enteroendocrine cells (EECs) are rare cells found along the intestinal mucosa and represent the most extensive endocrine system in the human body. EECs sense nutrients in the gut lumen and, in response, secrete various hormones that act locally or at a distance.¹ Enteroendocrine cells release numerous peptides including glucagon-like peptides 1 and 2 (GLP-1, GLP-2), peptide YY (PYY), gastric inhibitory polypeptide (GIP), secretin (SCT), cholecystokinin (CCK), ghrelin (GHRL), neurotensin (NTS), or somatostatin (SST), and amines such as serotonin (5-HT). Various dietary metabolites such as fatty acids generated by the processing of triglycerides or short-chain fatty acids produced by the fermentation of dietary fibers by the gut microbiota are detected by EECs, thereby modulating their activity. Enteroendocrine hormones emerged as essential regulators of energy homeostasis via their control of intestinal absorption, food intake and insulin secretion.^{1–3} Importantly, GLP-1 receptor agonists are already used in the treatment of diabetes and obesity. Thus, a better understanding of the differentiation and function of the EEC system could lead to innovative strategies to manipulate them and develop novel treatments for metabolic diseases.

Like all intestinal epithelial cells, EECs are actively renewed throughout life. They differentiate from intestinal stem cells located in the crypts and migrate out towards the villi. The proendocrine transcription factor (TF) *Neurog3*/*Ngn3* determines endocrine destiny and is essential for EEC differentiation in mice and humans.^{4–6} Single-cell transcriptomic studies also provided evidence that EECs express various hormones repertoires (rather than one hormone per EEC cell type) dynamically, from the small to large intestine and along the crypt-villus axis.^{7–12}

A constitutive lack of EECs induces lipid malabsorption. It demonstrates the critical role of enteroendocrine hormones in energy uptake and growth of neonate mice, which frequently die when born without EECs.¹³ Similarly, human newborns with mutations in *NEUROG3* lack all EECs in a condition termed “enteric anendocrinosis” and present with severe malabsorptive diarrhea requiring parenteral nutrition.¹⁴ A recent study by McCauley and colleagues shed light on the role of EEC hormones in linking nutrient sensing and absorption.¹⁵ Despite the role of EECs in lipid absorption, the transcriptomic program induced by lipids in EECs is poorly explored. Furthermore, in these studies,^{13,14} humans and mice with mutations in *NEUROG3* have impaired EEC development since birth. Therefore, the importance of the


EEC system in regulating energy homeostasis could not be addressed thoroughly in healthy adult mice because most mice with a constitutive EEC deficiency die in the first weeks of life. Consequently, potential adaptation mechanism to sustained malabsorption in adults could also not be identified. Growing evidence points towards the importance of the gut microbiota in digestion and intestinal absorption. Yet, the role of EEC-microbiota interactions in these processes and the pathogenesis of metabolic diseases are understudied. Herein, by blocking the formation of EECs in adult males, we aimed to investigate the EEC system’s function in maintaining energy homeostasis and unravel intestinal transcriptomic response to the lack of enteroendocrine hormones and in interaction with the gut microbiota.

Results

Weight Loss and Survival of EEC-deficient Mice is Diet-dependent

To address the role of EECs in maintaining energy homeostasis in healthy adult mice, we generated a tamoxifen-induced EEC depletion model (*Neurog3*^{lox/lox}; Villin-CreER^{T2} or *Neurog3*^{ΔAdInt} or EEC-deficient thereafter). Tamoxifen efficiently induced the deletion of the proendocrine transcription factor *Neurog3* along the gut and consequently the renewal of EECs is impaired (Figure 1A). This was evidenced by a dramatic decrease in transcripts encoding diverse hormone genes (Figure 1B) or enteroendocrine transcription factors. We noticed a residual expression of *Sct* or *Sst* in *Neurog3*-deficient small intestines (Figure 1B), unlikely resulting from the partial deletion of *Neurog3*, because low *Sct* expression was also seen in *Neurog3* null mice.¹³ *Sct* and *Sst* transcripts could thus result from their *Neurog3*-independent expression. ChromograninA, a pan-endocrine marker, or hormone peptides could not be detected in the intestinal epithelium supporting that enteroendocrine hormones are not produced (Figure 1C–F). Apart from the endocrine lineage, we did not observe any perturbation of other intestinal epithelial cell lineages – including goblet cells and Paneth cells (Figure 1G–H). We noticed shorter villi in the proximal small intestine but no effect in the distal small intestine or in the colonic gland length (Figure 1I–J). Crypt-villus organization and cell proliferation in the transit-amplifying zone were not altered upon induction of EECs loss (Figure 1K–L), and neither was the expression of the

Abbreviations used in this paper: ANOVA, analysis of variance; BH, Benjamini and Hochberg; CCK, cholecystokinin; CD, chow diet; DE, differentially expressed; EECs, enteroendocrine cells; GHRL, ghrelin; GIP, gastric inhibitory polypeptide; GLP, glucagon-like peptide; GS-MS, gas chromatography-mass spectrometry; HDL, high-density lipoprotein; HFD, high-fat diet; LDL, low-density lipoprotein; MCI, Mouse Clinical Institute; MS, mass spectrometry; NTS, neurotensin; OTUs, operational taxonomic units; PYY, peptide YY; RT-qPCR, reverse transcriptase-quantitative polymerase chain reaction; SCT, secretin; SST, somatostatin; TF, transcription factor.

 Most current article

© 2023 The Authors. Published by Elsevier Inc. on behalf of the AGA Institute. This is an open access article under the CC BY-NC-ND license (<http://creativecommons.org/licenses/by-nc-nd/4.0/>).

2352-345X

<https://doi.org/10.1016/j.jcmgh.2023.02.013>

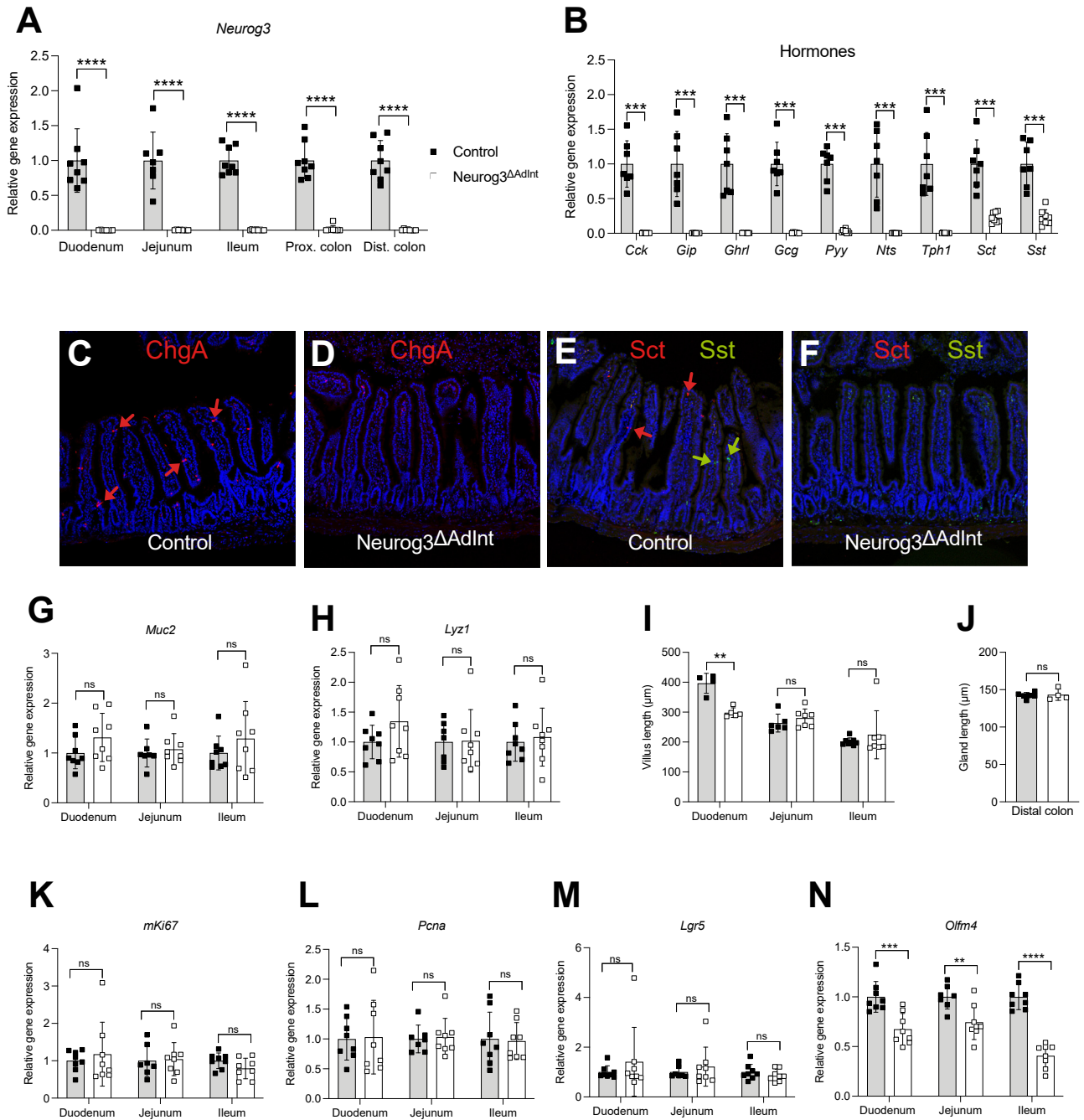


Figure 1. Induction of *Neurog3* deletion in the adult intestine precludes the differentiation of EECs but not of other epithelial cells. (A–B) Analysis, by RT-qPCR, of the expression of *Neurog3* (A) and transcripts encoding peptide hormones or *Tph1* (B), a marker of enterochromaffin cells, along the intestine and in the jejunum respectively, upon tamoxifen-induced *Neurog3* deletion. (C–F) Representative pictures of histo-immuno-fluorescence for Chromogranin A (ChgA) (red), somatostatin (Sst) (green), and secretin (Sct) (red) on cryosections (jejunum); nuclei are stained with DAPI (blue). (G–H) Analysis of goblet and Paneth cells markers by RT-qPCR for *Muc2* (G), *Lyz1* (H). (I–J) Morphometric analysis of villus length in the small intestine and gland length in the colon. (K–N) Analysis of proliferation and intestinal stem cell homeostasis by RT-qPCR for *mki67* (K), *Pcna* (L), *Lgr5* (M), and *Olfm4* (N). RT-qPCR data are normalized to control and represented as mean \pm SD; control males (black squares), *Neurog3*^{ΔAdInt} mutant males (open square); n = 8 for each genotype. Two-way ANOVA with Holm-Sidak posthoc comparisons (A, G, H, I, K–N) or Mann-Whitney test (B, J) with *P*-value > .05 (ns); < .05 (*); < .01 (**); < .001 (***); < .0001 (****) were performed for statistical analyses. Analyses were performed 18 weeks after tamoxifen administration. Tamoxifen was administrated at the age of 13 weeks.

stem cell marker *Lgr5* (Figure 1M). In contrast, *Olfm4*, another stem cell marker, was reduced (Figure 1N), which could result from the loss of Neurog3-positive endocrine progenitors, some of which co-express *Olfm4*.⁹

We previously showed that a constitutive lack of EECs is lethal for most CD1 outbreed newborn mutant mice.¹³ Surprisingly, we did not observe any death upon tamoxifen-induced EEC loss in adult Neurog3^{ΔAdInt} males fed with a standard chow diet (CD). On the contrary, 60% of EEC-deficient mice fed a high-fat diet (HFD) (lipids 60% kcal) died 5 weeks after tamoxifen administration. The remaining 40% of mice had to be sacrificed. Mice lost weight after EEC depletion under both CD and HFD (Figure 2A). The weight loss was immediate and worsened in Neurog3^{ΔAdInt} mice fed HFD. This weight loss was accompanied by an alteration in body composition (Figure 2B–G). Neurog3^{ΔAdInt} mice under a CD presented a decreased fat mass (–30%) and a higher lean mass (+6%) 10 weeks after the tamoxifen treatment (Figure 2B, C, E, F). This phenotype was exacerbated in EEC-deficient mice under an HFD, which showed a more significant and faster weight loss, starting from 1 week after tamoxifen administration (Figure 2A). This resulted in a similar but earlier alteration of the body composition seen in EEC-deficient mice fed a CD: a decreased fat mass (–57%) and an improved lean mass (+15%) as soon as 4 weeks after the tamoxifen treatment (Figure 2B–C). Accordingly, we observed an earlier decrease in body mass index in HFD nutrition conditions (Figure 2H–I). In summary, EECs are essential to sustain weight in adult males, especially under an HFD, suggesting a crucial role of enteroendocrine hormones in lipid assimilation in adults. Nevertheless, under a standard CD, weight loss was not life-threatening, suggesting that adult mice adapt following the depletion of EECs.

Lack of EECs in Adult Males Impairs Food Efficiency and Lipid Metabolism

Next, we investigated the progressive weight loss and energy imbalance in chow-diet fed mice following EEC depletion. Despite similar food intake compared with control littermates (Figure 2J), EEC-deficient mice produced more feces (Figure 2K). Measuring the residual energy contained in the stools by bomb calorimetry revealed an increase in excreted energy in feces of EEC-deficient mice (Figure 2L–M), suggesting poor assimilation of nutrients and implying a lower food efficiency (Figure 2N). The analysis of feces composition (Figure 3A–F) by mass spectrometry (MS) revealed increased quantities of cholesterol and its precursors, lathosterol and desmosterol, in EEC-deficient mice stools as soon as 3 weeks after tamoxifen treatment. The increased excretion of lipids was accompanied by significantly lower blood concentrations of total, high-density lipoprotein (HDL), and low-density lipoprotein (LDL) cholesterol, triglycerides, and free fatty acids in EEC-deficient mice, whereas glycerol levels were unchanged (Figure 3G–I, K–M). Taken together, increased cholesterol concentration in feces agrees with its plasmatic decrease and supports a deficit in cholesterol assimilation in mice

lacking EECs. Blood levels of bile acids were not affected (Figure 3N), suggesting in-range bile acids secretion and reabsorption. In contrast, the plasmatic concentration of lipase was decreased in mutants (Figure 3J), in agreement with the loss of CCK and SCT known to trigger lipase secretion from pancreatic acinar cells. These results suggest that decreased pancreatic lipase could alter the processing of dietary lipids and their absorption.

We assessed lipids' presence throughout the intestinal mucosa to further characterize lipid malabsorption. Under normal conditions, it has been reported that 95% of lipids are absorbed in the proximal small intestine,¹⁶ where the alimentary bowl mixes with bile acids and pancreatic lipase, aiding and performing lipids digestion. Oil red O staining of the EEC-deficient gut revealed fewer neutral lipids in the duodenum and more in the ileum compared with controls, suggesting less absorption in the proximal small intestine and lipid accumulation further away along the gut (Figure 3O–Q). In addition, the presence of neutral lipids in the intestinal lamina propria of EEC-deficient mice highlights that the transport of lipids in chylomicrons from the enterocyte to the lamina propria was not abolished. EEC-deficient animals suffer from lipid malabsorption characterized by higher feces production, higher excretion of non-assimilated energy/nutrients and, particularly, sterols in feces, lower plasmatic lipid levels, and a spatial delay of lipid absorption. Thus, EECs are necessary to uptake lipids in adult mice fed a CD.

Transcriptional Adaptation of the Small Intestine to Sustained EEC Deficiency

To gain further insights into the mechanisms underlying lipid malabsorption and to identify compensatory mechanisms for EEC loss and metabolic alterations, we explored the transcriptome of the proximal (duodenum) and distal (ileum) small intestine in the EEC-deficient and control mice (CD) (Figure 4). As expected, enteroendocrine markers such as hormone genes (*Gcg*, *Pyy*, *Tph1*, *Cck*, *Sct*, *Nts*, *Sst*, *Tac1*), EECs' GPCRs (*Ffar1*, *Adgrg4/GPR112*), granule components (*Chga*, *Chgb*, *Scgn*), and transcription factors controlling EEC differentiation downstream of *Neurog3* (eg, *Lmx1a*, *Neurod1*, *Rfx6*, *Isl1*, *Pax6*, *Nkx2-2*), were severely under-expressed in the Neurog3^{ΔAdInt} small intestine (Figure 4A–B). In addition, we found a decreased expression of several genes involved in lipid metabolism that could account for the malabsorption phenotype (Figure 4A–B). As an example, *Ces2a*, a carboxylesterase 2A with triglyceride hydrolytic activity¹⁷ was downregulated in the duodenum and ileum (Figure 4A–B). The expression of cytochrome P450, *Cyp2c29*, which has been shown to protect mice against HFD-induced obesity,¹⁸ *Fabp6*, which controls ileal bile acids absorption,¹⁹ and *Ces1g*, which regulates chylomicrons formation and inhibits their secretion,²⁰ are downregulated exclusively in the ileum (Figure 4B). Interestingly, the expression of the sterol efflux pump *Abca1*, proposed to mobilize membrane-free cholesterol for the formation of HDL particles that enter the lymphatic circulation, is downregulated in the proximal and distal small intestine

(Figure 4A–B),²¹ which might contribute to the lowering of blood cholesterol concentrations in EEC-deficient mice.

Overall, transcriptional changes between controls and EEC-deficient mice were more prominent in the ileum compared with the duodenum, with 598 vs 328 genes differentially expressed (DE), respectively (adjusted P value $\leq .05$; $|\log_2\text{FC}| \geq 0.5$). Between 16% and 24% of transcripts were similarly regulated in both intestinal segments. In comparison, other gene expression changes were specific to the duodenum or the ileum (Figure 4C–D). We used Gene Ontology analyses focusing on upregulated genes to reveal enriched adaptive biological processes (Figure 4E). Ontology terms related to lipid metabolism (eg, cholesterol biosynthesis, triglyceride metabolic process, metabolism of lipids) were enriched in the duodenum and ileum transcriptome, suggesting that lipogenic pathways were stimulated in EEC-deficient small intestine. For example, transcripts for the fatty acid transporter *Slc27a1*/FATP1 and the thyroid hormone-responsive gene *Thrsp* regulating de novo lipogenesis²² were increased in the duodenum and ileum. Other genes involved in lipogenesis (*Scd1*) and cholesterol metabolism (*Pcsk9*, *Ldlr*) were specifically upregulated in the duodenum^{22–24} (Figure 4A, D). The most significant fold change in the ileum was observed for *Pla2g4c*, which was strongly increased in EEC-deficient mice (Log₂FC = 6.4; adjusted P value = 1.36E–20). Little is known about this phospholipase in the intestine, but it has been suggested to enhance lipid droplet biogenesis in the liver.²⁵ We noticed an upregulation of *Creb3l3*/CREB-H, a transcription factor regulating triglyceride metabolism and induced by fasting,²⁶ of the lipogenic genes *Me1*²⁷ and fatty acid synthetase *Fasn* and its upstream regulator, the transcription factor *Mlxipl*/ChREBP,²⁸ and of *Acat2*, which esterifies sterols in enterocytes (Figure 4B, D).

In addition to genes involved in lipid metabolism, we also noticed an upregulation in the ileum of genes controlling carbohydrate metabolism (Figure 4B, D), such as the glucose (*Slc2a2*/GLUT2, *Slc5a1*/SGLT1) and fructose transporters (*Slc2a5*/GLUT5), the brush border enzyme sucrase-isomaltase (*Sis*), which hydrolyzes the dietary carbohydrates, and genes involved in intestinal gluconeogenesis (*Gls*, *Fbp1*). Importantly, many genes encoding antimicrobial proteins (*Ang4*, *Reg3b*, *Reg3g*, *Defa40*, *Defa3*, *Defa24*, *Sprr2a3*, *Retnlb*)^{29,30} were upregulated mainly in the duodenum, and genes encoding immunoglobulin chain (eg, *Ighv7-1*, *Igkv8-28*) increased throughout the small intestine. A similar upregulation of antimicrobial proteins (eg, *Reg2*, *Reg3b*, *Reg3g*, *Defa21*, *Defa22*) and immunoglobulin genes (*Igkv7-33*, *Igv14-100*) was observed in EEC-deficient mice fed an HFD (Figure 5A–B), suggesting that, in both diet conditions, a defense mechanism against microorganisms has been triggered, including stimulation of intestinal innate mucosal immunity. In contrast, *Slc2a2*, *Slc2a5* and *Sis*, were found to be upregulated under a regular diet in mice lacking EECs and were unchanged in HFD conditions, implying that the uptake and processing of carbohydrates are not promoted. However, increased *Glutaminase* (*Gls*) and *glucose-6 phosphatase* (*G6pc*) transcripts, in the duodenum, support intestinal gluconeogenesis.

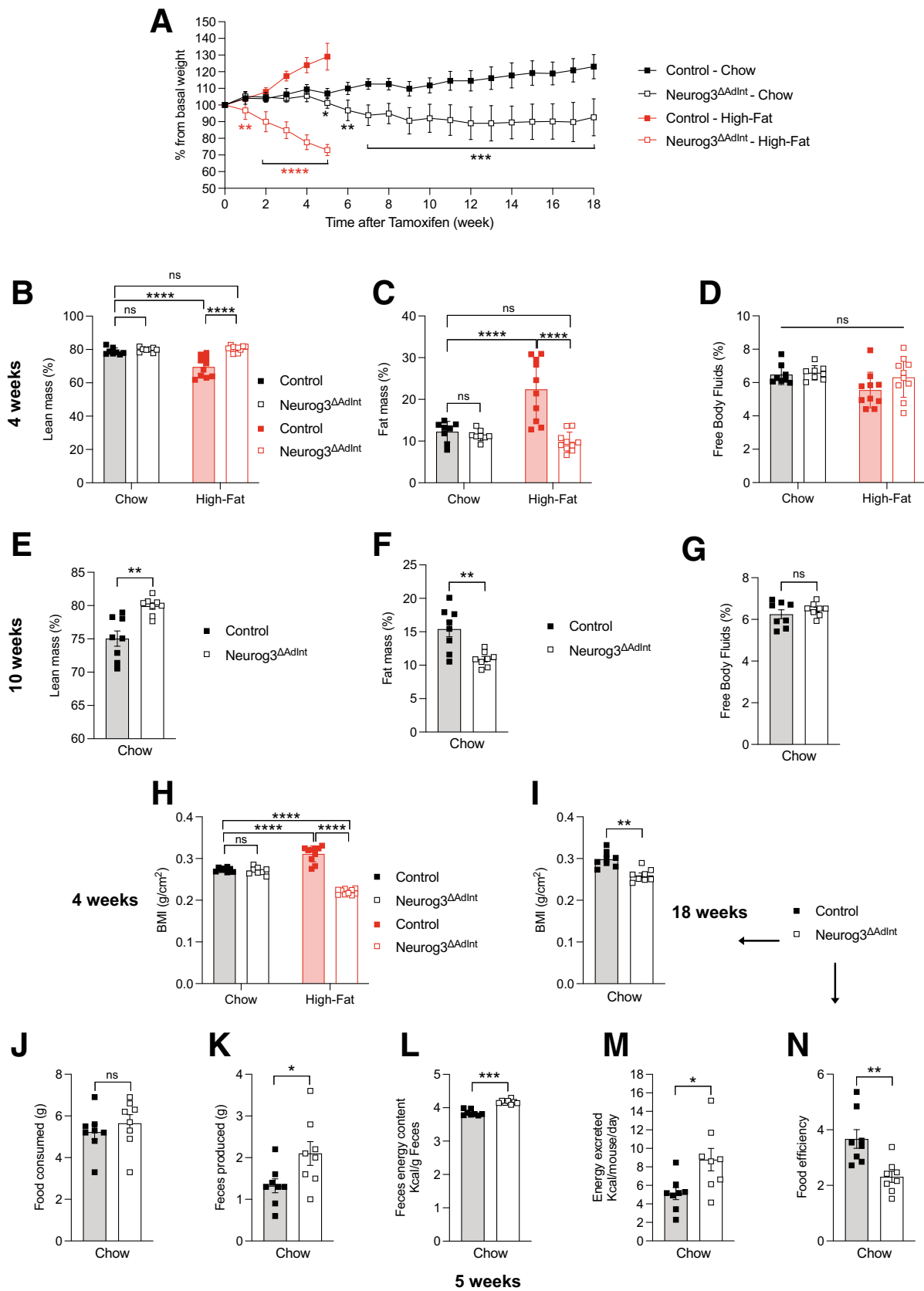
We hypothesize that, when fed a CD, EEC-deficient mice metabolism shifts towards an increased nutrient transport (carbohydrates, lipids), chylomicrons formation, lipogenesis, and gluconeogenesis to compensate for decreased food efficiency and lipid malabsorption. Under high-fat nutrition, enhancement of carbohydrate metabolism is limited to compensate for lipid malabsorption due to their low content in the diet. Interestingly, increased expression of antimicrobial peptides and genes related to immunity point out gut microbiota alterations.

HFD-induced Transcriptomic Changes in EECs

Given the vital function of EECs when mice are fed an HFD, we evaluated the impact of an HFD on EECs gene expression in response. Briefly, we compared the transcriptomic profiles of EECs sorted from the jejunum of mice fed with a standard CD or an HFD. Under a standard diet, the signature of EECs revealed 3835 genes DE (adjusted P -value $\leq .05$; $|\log_2\text{FC}| \geq 1$) compared with other intestinal epithelial cells (Figure 5C). EEC-enriched transcripts (compared with non-EEC) include known hormone genes such as *Ghrl*, *Tac1*, *Gcg*, *Sct* or TFs (*Insm1*, *Arx*, *Pax4*, *Rfx6*), as well as numerous uncharacterized genes related to EECs (eg, *Dgkb*, *C130021I20Rik*, *Rtn2*, *Usha2a*, *Vwa5b2*). Next, we evaluated transcriptional changes in EECs induced by an HFD (Figure 5D). We identified 853 genes DE (437 upregulated, 416 down-regulated) in EECs of mice fed with an HFD compared with the CD. Interestingly, 345 genes were exclusively upregulated by the HFD in EECs and not in other jejunal epithelial cells (blue points in Figure 5D). The transcripts for *Pyy*, *Sct*, *Cck*, *Nts*, *Gip*, and *Vgf* were increased in HFD conditions. Although the role of some of the corresponding hormones in lipid absorption has been previously reported, such as for NTS, CCK, and SCT,^{3,31} the function of GIP and VGF in response to luminal lipids nutrients is mainly unknown. Other genes involved in lipid metabolism were also upregulated, specifically in EEC, such as *Apoa5* which is almost exclusively expressed in the liver and controls chylomicron formation and triglyceride metabolism.^{32,33} Notably, the cyclooxygenase *Ptgs2*/*Cox-2*, required for the formation of prostaglandins from arachidonic acid, is strongly upregulated in EECs upon HFD. In agreement with the induction of prostaglandins, Monoglyceride lipase *Mgll*/*Magl*, the major enzyme hydrolyzing monoglycerides to glycerol and fatty acids, which also degrades the cannabinoid 2-arachidonoyl glycerol (2-AG) into arachidonic acid, was upregulated as well.³⁴ Similarly, the Hemopexin transcripts (*Hpx*), a gene not expressed in EECs under the CD, but regulated in mouse adipose tissue by HFD or the transcription factor *Prrx2* were found to increase.³⁵ In summary, analysis of EEC transcriptomic response to an HFD revealed the upregulation of a subset of hormone-encoding mRNAs as well as of genes involved in lipid metabolism and specifically induced in EEC.

Remodeling of Intestinal Microbiota After EEC Loss

We hypothesized that intestinal malabsorption and antimicrobial response following EEC depletion could reflect an altered microbiota composition. We thus



compared the gut microbiota using 16S rRNA-sequencing of mouse feces, before and 15 and 30 days after the induction of EEC deletion in the adult gut (Figure 6). The analysis of the fecal microbiota revealed a progressive decrease in α -diversity with a reduction of richness and Shannon indexes over time in the feces of EEC-deficient mice (Figure 6A). The analysis of β -diversity, measured by Bray-Curtis metrics, revealed significant differences in the microbiota of EEC-deficient mice at 30 days compared with control (Figure 6B) (P -value = .001; PERMANOVA using Adonis function). Next, we identified the gut microbiota composition at different taxonomic levels (Figure 6C). Interestingly, although the dominant taxa remained stable in controls over time, comparing the fecal microbiota composition before and 30 days after EEC loss in Neurog3^{ΔAdInt} mice revealed alterations affecting all taxonomic levels, from phyla to genera (Figure 6D–H). Indeed, even if *Bacteroidota* and *Firmicutes* phyla dominate the gut microbiota in controls and mutants, *Actinobacteriota* and *Proteobacteria* were enriched progressively in the feces of EEC-deficient mice as early as day 15 (Figure 6D). Nevertheless, the *Firmicutes* to *Bacteroidota* ratio, whose modification is commonly linked with obesity (increased ratio) or inflammation (decreased ratio), was not significantly affected (Figure 6E).³⁶

At the family level, EEC loss led notably to a severe reduction of *Muribaculaceae* and *Lachnospiraceae* and an enrichment in *Bacteroidaceae*, *Lactobacillaceae*, *Bifidobacteriaceae*, *Tannerellaceae*, *Atopobiaceae*, and *Sutterellaceae* (Figure 6F). In addition to the reallocation of the dominant families, we observed a modification of the relative abundances at the genera level (Figure 6G–H). Despite the interindividual differences (Figure 6G), the dysbiosis observed in Neurog3^{ΔAdInt} animals shares common features (Figure 6H). Differential abundance analysis between control and EEC-deficient mice revealed that several operational taxonomic units (OTUs) are over- or under-represented in mutant feces (Figure 6I). Among the significantly under-represented genera in mutant microbiota, we found notably several OTUs belonging to the genera *Lachnospiraceae* and *Prevotellaceae*, *Rikenella*, *Akkermansia*, *Muribaculum*, and *Desulfovibrio*. In parallel, OTUs associated with *Bacteroides*, *Lactobacillus*, *Bifidobacterium*, and *Osseella* genera, among others, were over-represented in mutant feces. Surprisingly, even though the main producers of short-chain fatty acids in the healthy gut, *Lachnospiraceae* and *Ruminococcaceae*, are impoverished in the feces of EEC-deficient mice, MS analysis did not reveal any change in the

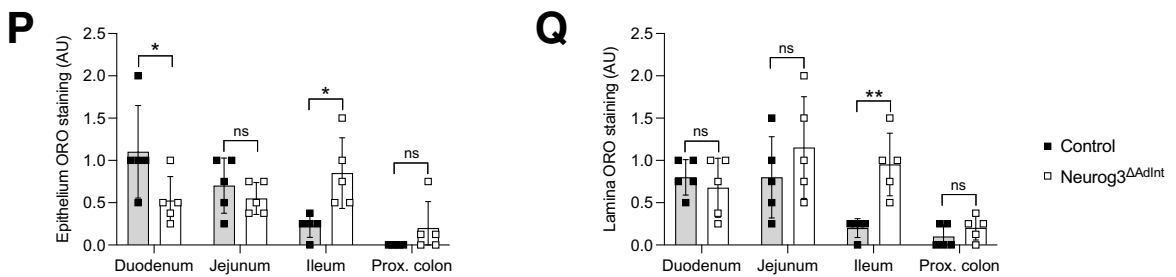
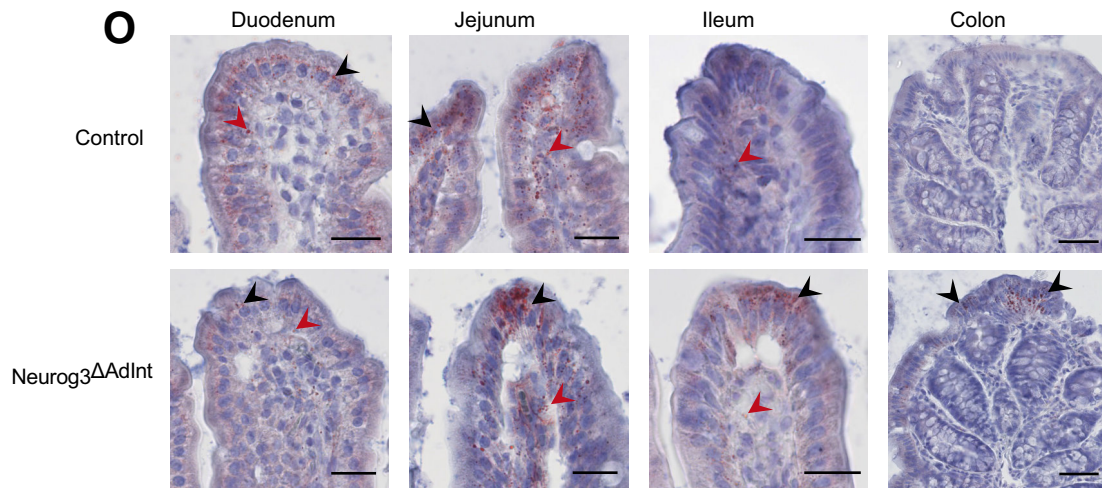
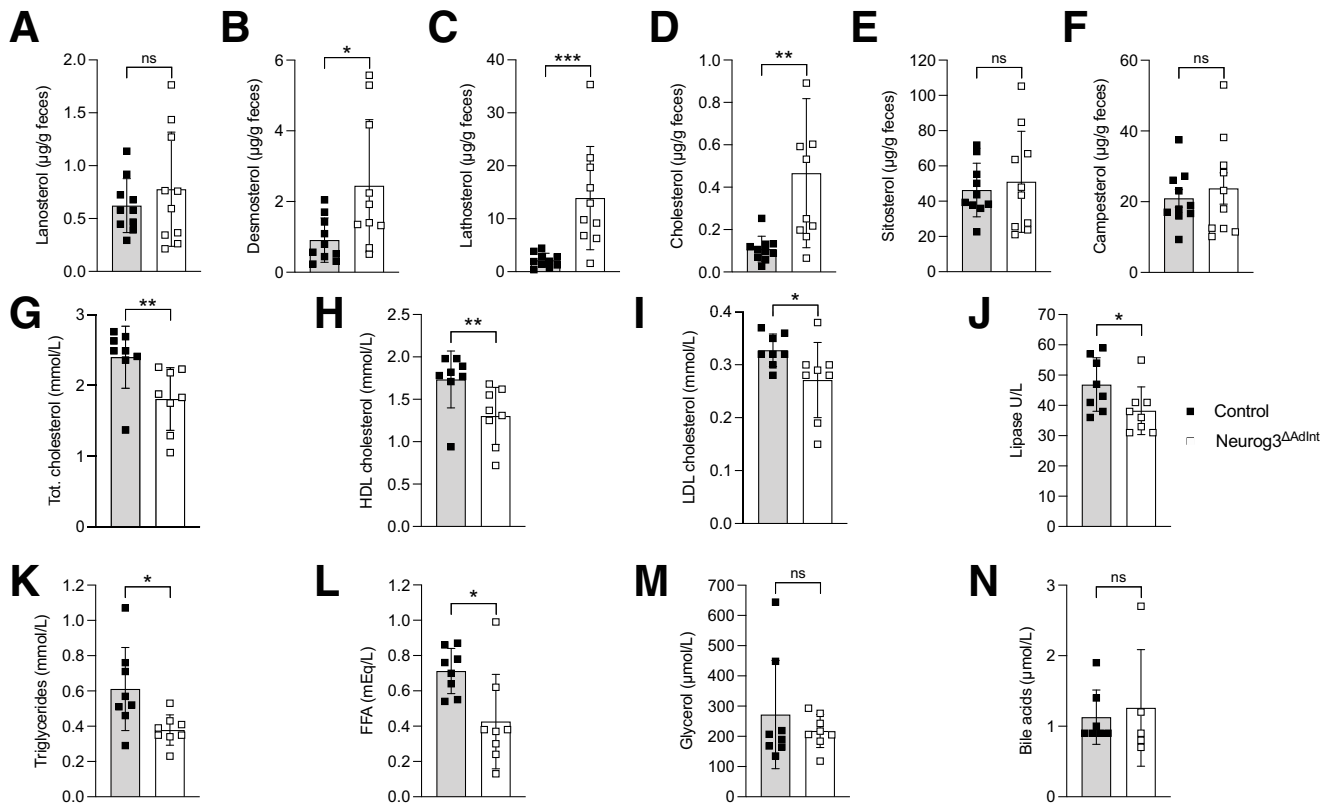
fecal concentration of short-chain fatty acids, including propionate, acetate, butyrate, isobutyrate, and valerate (Figure 7A). To further investigate the metabolic alterations associated with the taxonomic changes in the fecal microbiota of EEC-deficient mice, we inferred the predictive functional pathways using PICRUSt2. Twenty-five functional pathways were identified as significantly different between controls and EEC-deficient mice (Figure 7B–C). Among them, the relative abundance of 6 inferred pathways related to bacterial motility, antimicrobial resistance, secondary metabolites biosynthesis, and transcription machinery were higher in controls. EEC-deficient mice displayed an increased abundance of predicted pathways associated mainly to carbohydrate metabolism, energy metabolism, and xenobiotics degradation. Also, the relative abundance of pathways related to infection was higher in mutants compared with control mice. In summary, removing of EECs induced a progressive and severe alteration of the gut microbiota taxonomy and likely metabolism.

Discussion

The role of enteroendocrine hormones in energy homeostasis has been investigated using knockouts of individual hormone genes or receptors. However, the importance of the intestinal enteroendocrine system in healthy adult mice remains unknown. Our study describes physiological and intestinal transcriptional adaptative responses to a long-term, global, EEC depletion. We found impaired lipid malabsorption and food efficiency. Yet, EECs are dispensable for survival when mice are fed with a standard CD but are required when a lipid-enriched diet is given. We reported a rapid remodeling of the intestinal microbiota upon EECs removal, steady lipid malabsorption, and adaptative metabolic and transcriptomic responses. In addition, we provided novel insights into the role of EECs in lipid metabolism by unveiling EEC transcriptional response to an HFD, which revealed an increased expression of a subset of hormones transcripts and other regulators of lipid metabolism. All experiments have been performed in males; we thus cannot conclude whether EEC-deficient female mice have a similar phenotype.

After induction of EEC deficiency, we first noticed that mice lost weight. However, when fed with an HFD, the weight dropped severely, and experimentation needed to be stopped. This observation agrees with the failure to thrive and the death of most murine neonates with intestinal EEC-deficiency when fed with high fat-containing mother's

Figure 2. (See previous page). **Progressive weight loss and decreased food efficiency in mice lacking EECs.** (A) Evolution of weight after tamoxifen administration in control and Neurog3^{ΔAdInt} males fed a CD (black symbols) or HFD (red symbols). (B–G) Proportion of lean mass (B, E), fat mass (C, F), and free body fluids (D, G) relative to body weight, respectively, 4 or 10 weeks after the tamoxifen treatment. (H–I) Body mass index (BMI) 4 or 18, respectively, weeks after tamoxifen administration. (J–K) Measure of food intake (J), feces production (K). (L–N) Evaluation of fecal residual energy (L), daily energy excreted (M), and food efficiency (N) (energy ingested/energy excreted) under CD. Feces energy content was evaluated by calorimetric bomb. Measures were taken 5 weeks after tamoxifen administration. Data are represented as mean \pm SD, controls (full squares), Neurog3^{ΔAdInt} mutants (open squares); $n = 8$ under CD (black); $n = 10$ under HFD (red), males. Two-way ANOVA with Holm-Sidak post-hoc comparisons (A–D, H), Mann-Whitney test (E–G, I–N) with P -value $> .05$ (ns), $< .05$ (*), $< .01$ (**), $< .001$ (***), $< .0001$ (****); in (A) comparisons are performed within each diet; significant differences are represented with a black asterisk under CD and red asterisk under HFD.



milk.¹³ Interestingly, *Rfx6*^{ΔAdInt} mice,¹² which lack all EECs except enterochromaffin cells, only transiently lost weight. Despite lipid malabsorption, these mice caught up rapidly with wild-types, suggesting that serotonin/5-HT prevented weight loss, by promoting stored energy release.³⁷ This might explain the more pronounced phenotype in *Neurog3*^{ΔAdInt} compared with *Rfx6*^{ΔAdInt} mice. Bomb calorimetry experiments revealed decreased food efficiency in EEC-deficient mice, likely resulting from lipid malabsorption. We found that lipid absorption was spatially delayed and increased in the ileum 1 month after EECs removal. A similar distal shift of lipid absorption was observed in another mouse model of extensive EEC deficiency.³⁸ It could be a compensatory mechanism for the duodenal malabsorption resulting from EEC deficiency.

To identify the mechanisms underlying lipid malabsorption and adaptative responses of EEC-deficient mice fed a CD, we profiled the transcriptome of their duodenum and ileum and scrutinized the expression of known regulators of the different steps of lipid absorption.²¹ Although the expression of important fatty acid and cholesterol absorption regulators were unchanged in EEC-deficient mice, we found that transcripts of proteins involved in chylomicrons formation (*Apob*/*Apob-48* or *Ces1g*), ileal bile acids absorption (*Fabp6*) or cholesterol uptake (*Abca1*) were decreased in EEC-deficient mice. Also, blood concentrations of lipase, whose secretion is stimulated by CCK and SCT enteroendocrine hormones, were decreased in EEC-depleted mice, suggesting triglyceride hydrolyses could be impaired. Thus, lipid malabsorption in EEC-depleted mice might result from combined alterations of fat digestion by lipase, fatty acid and cholesterol transport, and chylomicron lipoprotein assembly.

We next focused on upregulated genes to identify possible adaptation mechanisms implemented in EEC-deficient mice to improve energy homeostasis. In the duodenum, increased expression of *Scd1*, *Pcsk9*, and *Ldlr* suggested lipogenesis and cholesterol uptake to be stimulated. Upregulated genes were numerous in the ileum. Notably, *Pla2g4c*, the top gene strongly enriched in the EEC-deficient ileum, encodes the phospholipase A2 gamma, recently shown in a human hepatocellular carcinoma cell line to promote lipid droplet formation.²⁵ However, such a function was so far not reported in enterocytes. Another gene highly enriched is the cilia and flagella-associated protein 61, *Cfap61*. Of note, cilia have been shown to drive adipogenesis through ciliary signaling in preadipocytes.³⁹ Stimulation of

enterocytic lipid resynthesis could be another compensatory mechanism, owing to the ileal increased expression of the acyl-CoA cholesterol acyl transferase *Acat2*, known to esterify sterols in enterocytes' endoplasmic reticulum.⁴⁰ Notably, transcriptome analysis also suggested that carbohydrate metabolism and intestinal gluconeogenesis is promoted in the ileum of EEC-deficient mice. Transcriptional adaptation in the ileum might result from the upregulation of the lipogenic and glycolytic transcription factor *Mlx1pl/ChREBP*, thought to integrate metabolic signals to modulate its activity according to nutritional status.⁴¹ Thus, intestinal transcriptomic alterations in EEC-deficient mice reflect the lack of enteroendocrine secretion and impaired lipid metabolism and adaptative responses promoting lipogenesis and carbohydrate metabolism to overcome lipid malabsorption failures and improve energy homeostasis. Importantly, the dramatic weight loss of EEC-deficient mice fed an HFD could result from their limited possibility to shift to carbohydrates as an alternative energy source. Indeed, the transcriptomic analysis revealed that the expression of genes controlling the uptake and processing of dietary carbohydrates are not enhanced unlike CD nutrition conditions.

The phenotyping of mice lacking EECs and corresponding hormones confirmed the role of enteroendocrine hormones in lipid metabolism. However, we profiled their transcriptome in wild-type mice to gain further insights into EEC's response to an HFD. We found that transcripts for *Pyy*, *Sct*, *Cck*, *Nts*, *Gip*, and *Vgf* hormones were increased, suggesting the need to overproduce them to compensate for a high-fat intake. These findings suggest a previously unappreciated role of GIP and VGF in EEC response to lipids. Indeed, the function of GIP in lipid metabolism has not been extensively studied, but recent findings report that GIP receptor-deficient mice, fed an HFD, have reduced adiposity.⁴² VGF is co-expressed with serotonin in intestinal enterochromaffin cells.¹² Hypothalamic VGF is important for appetite regulation and VGF-deficient mice have reduced stored lipid in white adipose tissue.⁴³ Nevertheless, the role of intestinal VGF and derivative peptides is unknown. Besides hormone transcripts, we also found that genes involved in lipid metabolism (*ApoA5*, *Ptgs2/Cox2*, *Mgll1/Magl1*) were upregulated specifically in EECs in HFD conditions but not in other intestinal epithelial cells. In summary, we established the transcriptomic signature of EECs in response to an HFD, thereby generating novel hypothesis on their specific role in lipid metabolism.

Figure 3. (See previous page). Impaired and spatially delayed lipid absorption in EEC-deficient mice. (A–F) Dosage of fecal sterols by gas chromatography-mass spectrometry, 3 weeks after tamoxifen administration. (G–N) Blood concentrations of total cholesterol (G), HDL cholesterol (H), LDL cholesterol (I), lipase (J), triglycerides (K), free fatty acids (FFA) (L), glycerol (M), and bile acids (N) 18 weeks after tamoxifen administration in controls and *Neurog3*^{ΔAdInt} males under CD. (O–Q) Evaluation of lipid absorption by Oil Red O (ORO) staining 1 month after Tamoxifen administration; O, Representative staining of intestine cryosections with ORO in red; nuclei are counterstained with hematoxylin. Scale bars: 25 μm in duodenum, jejunum, and ileum; 50 μm in proximal colon. Red arrows indicate fat droplets in the lamina propria, and black arrows point to vesicles in the epithelium. Slide scanner Hamamatsu, Nanosizer 2.0 HT. (P–Q) Quantification of fat droplets in the epithelium (P) and lamina propria (Q). Data are represented as mean ± SD, controls (black squares), *Neurog3*^{ΔAdInt} mutants (open squares); n = 10, 8, and 5 animals per genotype in (A–H), (I–N), and (O–Q) respectively. Mann-Whitney test with P-value > .05 (ns), < .05 (*), < .01 (**), < .001 (***), < .0001 (****) in (A–N). Two-way ANOVA with Holm-Sidak post-hoc comparisons with P-value > .05 (ns), < .05 (*), < .01 (**), < .001 (***) in P–Q.

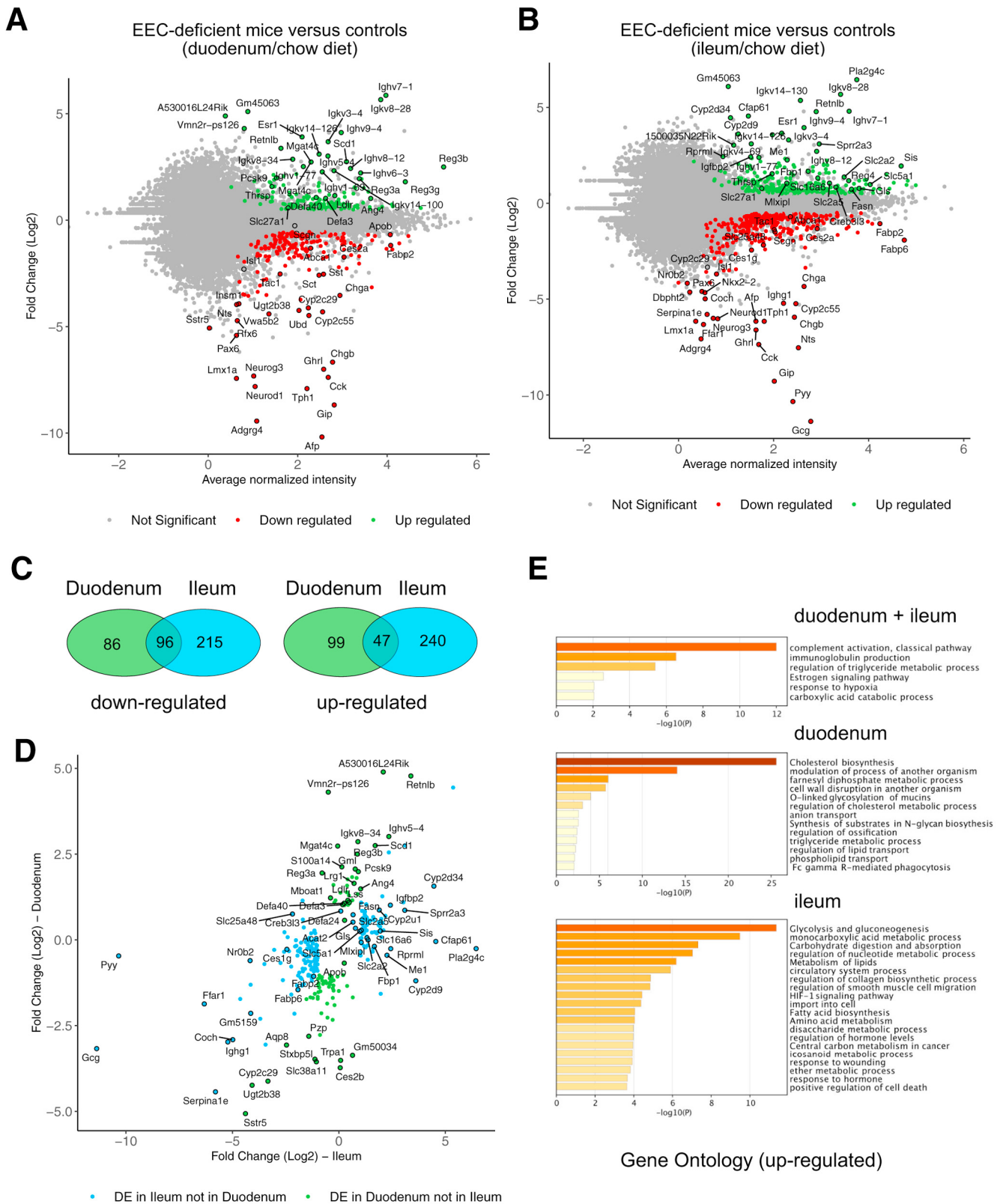


Figure 4. Transcriptional response to EEC loss in the proximal and distal small intestine in mice fed a CD. (A–B) MA plots illustrating RNA-Seq analysis of the duodenum (A) or ileum (B) of EEC-deficient mice compared with controls (CD); a selection of genes is highlighted. (C) Venn diagrams depicting overlapping and duodenum- or ileum-specific DE genes in EEC-deficient mice compared with controls. (D) Genes DE in the duodenum and not in the ileum of EEC-deficient mice compared with controls (green dots) and vice versa (blue dots). (E) Gene Ontology terms enrichment (Metascape) for up-regulated genes are shown. In A and B, MA plots represent the estimated Log2 fold change as a function of the mean of normalized counts in A and B; in D, Log2 fold change are plotted for a selection of genes DE in the duodenum and ileum. Genes with an adjusted P -value $\leq .05$ and $|\log_2FC| \geq 0.5$ were selected for the analysis; $n = 4$ mice per genotype.

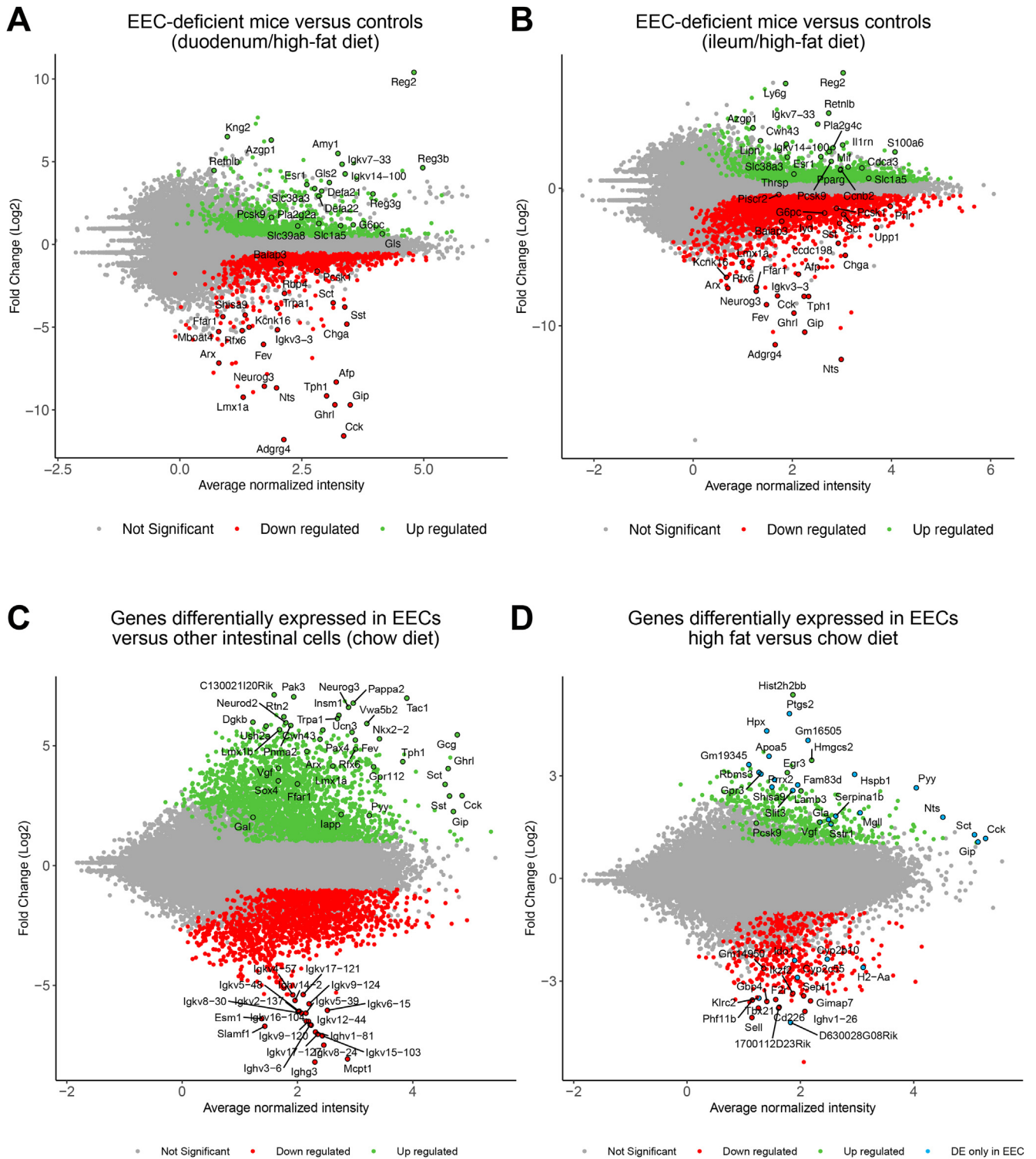
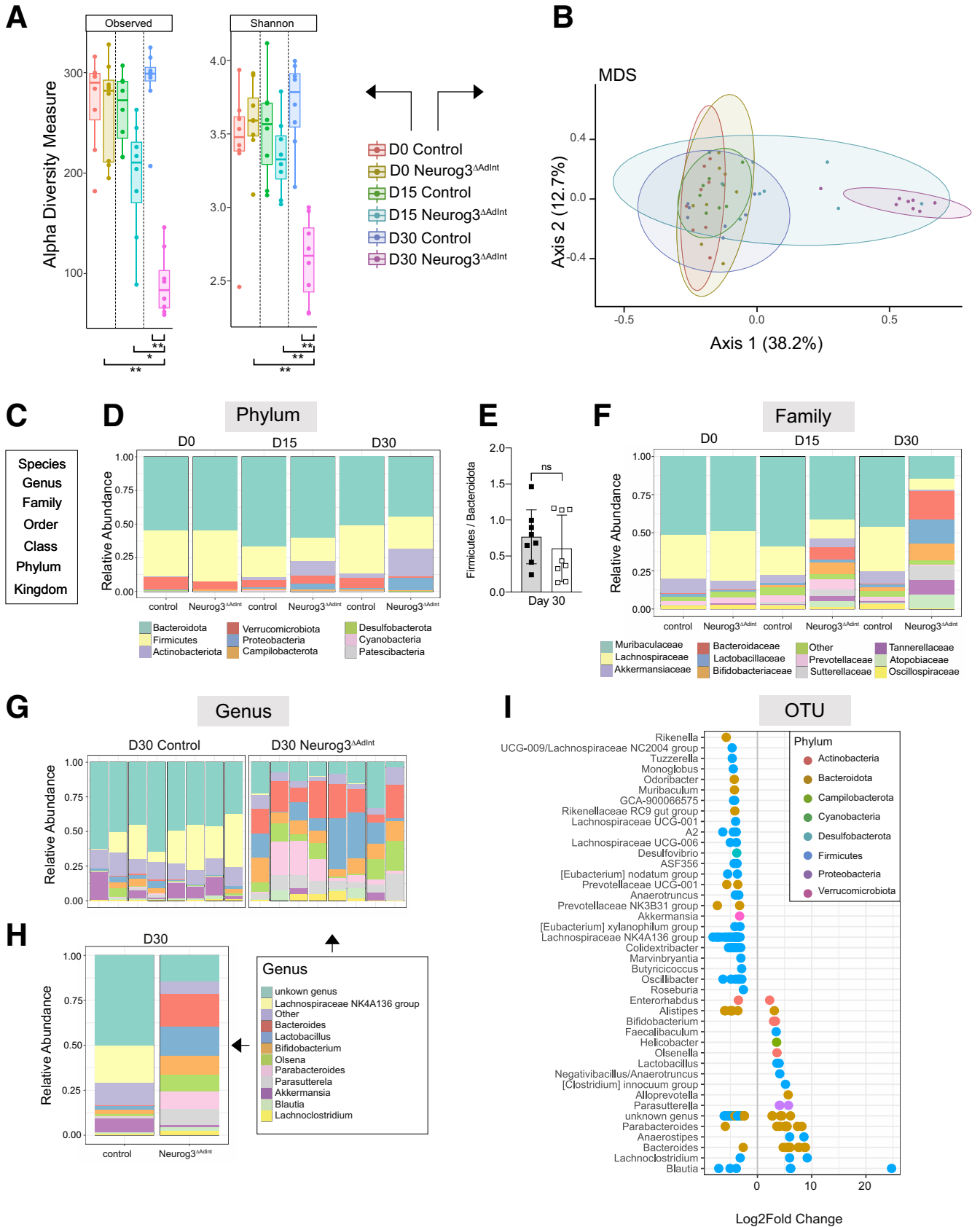


Figure 5. Transcriptional response to EEC loss in the proximal and distal small intestine in mice fed an HFD and HFD-induced genes in EECs. (A–B) MA plots illustrating RNA-Seq analysis of the duodenum (A) or ileum (B) of EEC-deficient mice compared with controls (fed HFD). (C) MA plot illustrating RNA-Seq analysis of EECs (eYFP-positive) and non-EECs (eYFP-negative) purified from villi of jejunum of *Neurog3^{eYFP}* jejunum mice (12 weeks) fed with a regular CD. (D) MA plot showing genes differentially expressed in eYFP-positive EECs sorted from the jejunum of *Neurog3^{eYFP}* mice (12 weeks) fed with a standard CD or HFD (during 4 weeks). The excellent stability of the eYFP protein allows the labeling and sorting of endocrine progenitors and mature EECs. MA plots represent the estimated Log₂ fold change as a function of the mean of normalized counts. A selection of genes DE are highlighted in (A–D). Green and red points represent significantly (adjusted *P*-value ≤ .05) up- and down-regulated genes (log₂FCI ≥ 0.5 (A, B) or 1 (C, D); n = 4 mice per genotype (A, B) or n = 3 (C, D) per condition. Blue points in D represent a selection of genes that are specifically up-regulated in EECs and not in other non-EECs by an HFD.



The gut microbiota is an essential regulator of nutrient digestion, absorption, and energy harvest.^{44,45} Alterations of gut microbiota have been shown in diverse metabolic diseases.⁴⁶ Various metabolites, including short chain fatty acids and products of dietary fiber fermentation, mediate its metabolic role. Short-chain fatty acids serve as an energy source but can also signal via fatty acid receptors at the surface of EECs modulating both their hormonal secretion^{47,48} and transcriptome.⁴⁹ Whether, in turn, enteroendocrine hormones influence microbiota composition has not been studied directly. Analysis of the microbiota in the stools of mice lacking EECs and fed a regular chow diet revealed a severe drop in alpha and beta-diversity, 4 weeks after the induction of EECs depletion and before weight loss. *Bacteroides* and *Lactobacillus* were found progressively enriched, whereas several Firmicutes genera including *Lachnospiraceae* and *Muribaculaceae* decreased. An increase in gram negative bacteria *Proteobacteria* was also observed in EEC-deficient mice. Microbiota remodeling in EEC-deficient mice could be either causal to lipid malabsorption or secondary to gut dietary content changes due to residual unabsorbed lipids, which would favor the growth of subsets of bacteria. Indeed, the diet is essential for microbial composition as both starvation⁵⁰ and HFD^{51–53} have been shown to impact microbiota communities. For instance, HFD decreased *Bacteroidetes*, whereas *Firmicutes* and *Proteobacteria* increased.⁵² The *Firmicutes/Bacteroidetes* ratio was, however, unaltered in mice lacking EECs and fed with a CD. Thus, despite possible increased lipids in the gut lumen, microbiota changes differ from those reported in an HFD. Like mice lacking all EECs, this increased *Firmicutes/Bacteroidetes* ratio was also not observed in mice lacking neurotensin, which actually attenuated HFD-induced intestinal dysbiosis. Like EEC-deficient mice, neurotensin-deficient mice have reduced intestinal fat absorption.^{54,55} Changes in gut microbiota composition may result from changes in the host ecosystem such as transit time, pH. Studies suggest that *Firmicutes* and *Proteobacteria* are more tolerant to these factors.⁵⁶

Interestingly, the expression of genes encoding antimicrobial proteins such as *Reg3b*, *Reg3g*, or their upstream regulator *Retlnb*⁵⁷ was increased in the small intestine of EEC-deficient mice (both in CD and HFD). These antimicrobial peptides can be activated by intestinal bacteria to promote the spatial segregation of the microbiota from the epithelium.⁵⁸ Interestingly, alteration of the microbiota composition can induce increased expression of *Reg3g*, which is required for microbiota beneficial effect on body weight and energy balance.⁵⁹ Higher levels of antimicrobial

peptides in the duodenum could also suggest an increase in bacterial load in the duodenum of EEC-deficient mice. Lipid malabsorption and an increased intestinal anti-microbial response were also reported in mice lacking Arx transcription factor, which is necessary for the specification of Sct-, Cck-, Glp1-, Glp2-, Pyy-, Nts-, and Gip-expressing cells.³⁸ Despite the severe alteration of gut microbiota diversity in EEC-deficient mice, fecal short chain fatty acids were unaltered. Recent studies suggest that the small intestinal microbiota adapts to dietary lipid variations and plays an important role in lipid digestion and absorption.⁴⁵ Whether microbiota communities and their metabolites are modified in the small intestine of EEC-deficient mice remains to be explored.

We further investigated the metabolic alterations of EEC-deficient mice using PICRUST2 approach to predict the functional capability of their microbiota. The loss of EEC induced a decreased ability to maintain bacterial homeostasis as indicated by a lower abundance of pathways involved in chemotaxis, bacterial motility, and biosynthesis of antimicrobial products (beta-lactams and ansamycins). This suggests that the gut microbiota of EEC-deficient mice may have a lower fitness that could predispose to later infection.⁶⁰ Among different factors, the nutritional quality of the carbon source could participate in the alterations of these biological processes.⁶¹ The loss of EEC likely led the gut microbiota of EEC-deficient mice to shift towards increasing carbohydrate metabolism, including gluconeogenesis and lipoic acid metabolism, to find another source of carbon and energy. Interestingly, a metabolic shift towards carbohydrate metabolism was also suggested by the mouse transcriptomic data. Metabolic adaptation of the gut microbiota may participate in host adaptation following tamoxifen treatment. Also, inferred xenobiotic degradation pathways (aminobenzoate degradation, chlorocyclohexane and chlorobenzene degradation, nitrotoluene degradation) were over-represented in mutant mice. They may witness an increase in toxic compounds and optimization of energy source availability. Several predictive pathways (glutathione metabolism, selenocompound metabolism, and lipoic acid metabolism) increased in EEC-deficient mice were related to redox homeostasis balance and may participate in metabolic deregulation and oxidative stress.⁶² In particular, glutathione has been reported to affect bacterial pathogenesis and virulence.⁶³ In summary, the predictive functional analysis highlighted the alteration of several metabolic pathways that participate in both gut microbiota and host

Figure 6. (See previous page). Microbiota changes in mice lacking EECs. (A) Alpha-diversity was estimated by the richness (observed OTUs) and the Shannon index of bacterial communities in feces before (D0), and 15 (D15) and 30 days (D30) after tamoxifen treatment of control and Neurog3^{ΔAdInt} mice. Pairwise comparisons using Wilcoxon rank-sum test with P -value < .05 (*) and < .01 (**). (B) Plot of metric multidimensional scaling (MDS) analysis using Bray-Curtis dissimilarity between control and Neurog3^{ΔAdInt} mice. (C) Representation of the taxonomic levels. (D) Mean relative abundances of bacterial phyla in control and Neurog3^{ΔAdInt} mice over time. (E) Firmicutes to Bacteroidetes ratio in control and Neurog3^{ΔAdInt} mice at D30. Data are represented as mean ± SD. Statistical analyses were performed with the Mann-Whitney test; $P > 0.05$ (ns). (F) Mean relative abundances of bacterial families in control and Neurog3^{ΔAdInt} mice over time. (G–H) Relative abundances of bacterial genera in control and Neurog3^{ΔAdInt} mice over time per individual (G) and mean relative abundances per genotype at D30 (H). (I) OTUs were significantly different at the OTU level between Neurog3^{ΔAdInt} and control mice according to DESeq2 analysis. Data are represented as Log2 fold-change (FC) between Neurog3^{ΔAdInt} and control animals: log2FC > 0 means enriched in Neurog3^{ΔAdInt} mice. D0, D15, and D30 mean days 0, 15, and 30. $n = 8$ males per genotype under a CD; aged of 13 weeks at D0.

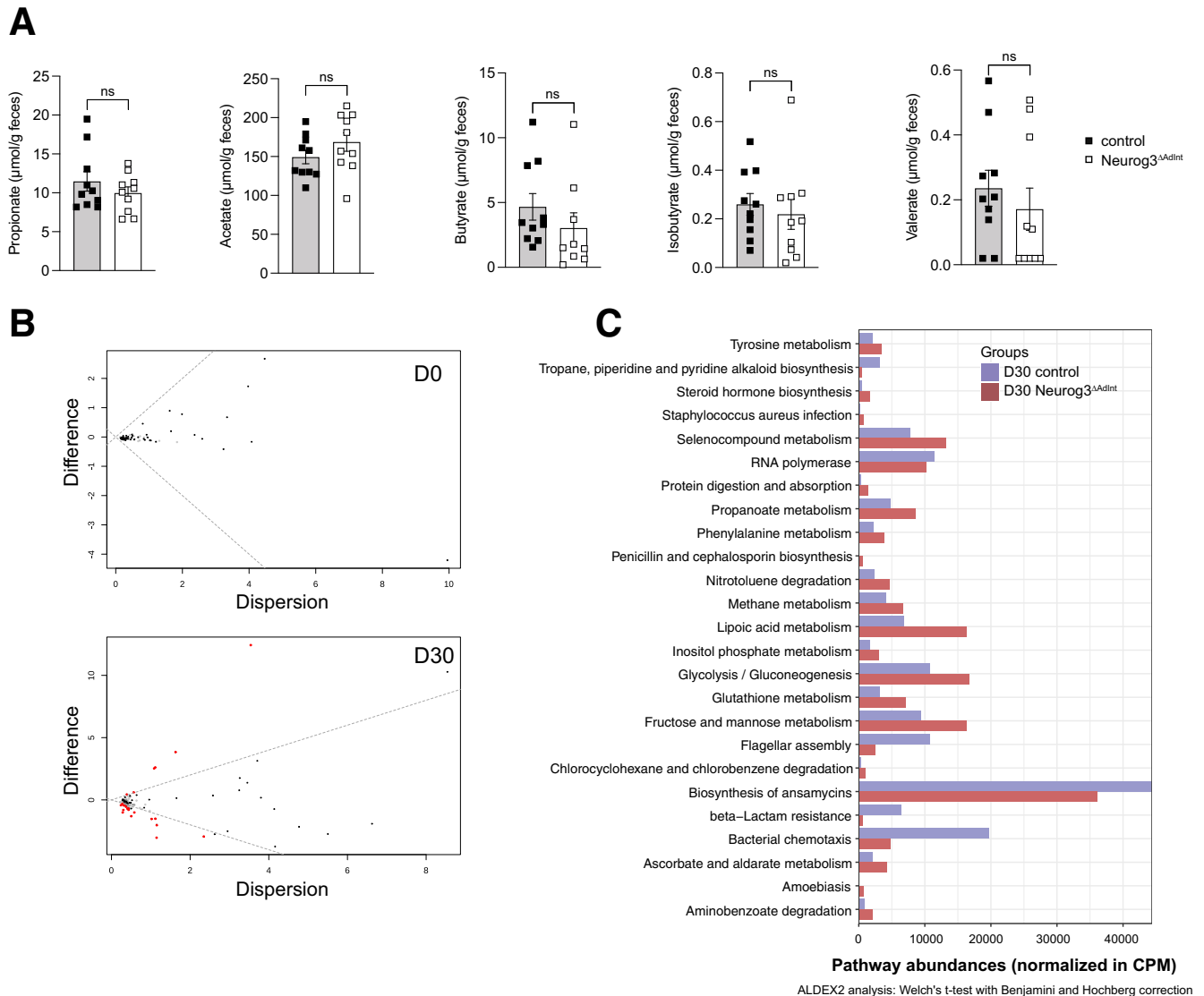


Figure 7. Analysis of microbial (microbiota-derived) metabolites and predictive functional pathways. (A) Concentration of short-chain fatty acids excreted in feces quantified by GC-MS 3 weeks after tamoxifen administration. Data are represented as mean \pm SD, controls (black squares), Neurog3 Δ AdInt mutants (open squares); $n = 10$ males per genotype; Mann-Whitney test with P -value $> .05$ (ns), $< .01$ (**), $< .001$ (***) . (B) MA plot of inferred microbial pathways predicted with PICRUSt2 between controls and Neurog3 Δ AdInt mutants, before (D0, upper panel) and 30 days (D30, lower panel) after tamoxifen treatment. Red dots show significantly altered pathways in controls (up) and Neurog3 Δ AdInt mutants (down). (C) Bar plot of Kyoto Encyclopedia of Genes and Genome (KEGG) predictive pathway abundance between controls and Neurog3 Δ AdInt mutants, 30 days after tamoxifen treatment. Only statistically different pathways according to the ALDEX2 test were reported. CPM, Count per million reads.

adaptation to the loss of EEC. However, it is still challenging to discriminate the pathways that compensate for the loss of energy source availability from pathogenic processes.

Overall, our studies show that in adult mice: (1) EECs are not essential for survival when mice are fed with a standard CD but are vital under high-fat nutrition, which triggers EEC-specific transcriptional changes in wild-type mice; (2) EECs are essential to optimize lipid absorption and food efficacy and maintain weight under a standard diet; (3) in the absence of EECs, intestinal lipid absorption is spatially delayed, and transcriptional changes suggest adaptation mechanisms to remedy lipid malabsorption and adjust energy utilization; (4) blocking EEC formation rapidly leads to

a severe drop of gut microbiota diversity and remodeling. These studies using mouse models may contribute to shedding light on the pathophysiology of human anendocrinosis and adaptive mechanisms that could be targeted to improve intestinal malabsorption and limit the need for parenteral nutrition.

Material and Methods

Study Approval

All animal studies were approved by the French Ministry of "Enseignement supérieur de la Recherche et de l'Innovation" ethical committee, in compliance with the European

legislation on care and use of laboratory animals (agreement no. APAFIS#22786-2019111511478935 v3).

Animals and Animal Handling

Mice had ad libitum access to water and 2 different types of diets from weaning: standard CD (Safe D04 diet – Safe Diets) or a rodent HFD with 60 kcal % fat (D12492 – Research Diets). Animals were maintained on a 12-hour light/dark cycle.

Inducible intestine-specific Neurog3-deficient mice, Neurog3^{ΔAdInt}, were generated by crossing Neurog3^{flox/flox} mice¹³ with the Villin-Cre^{ERT2} line⁶⁴ (gift of Dr S. Robine). Mice were maintained on C57BL/6 background. Genotyping was performed as previously described.¹³ In all this study, Neurog3^{flox/flox}; Villin-Cre^{ERT2} animals were referred to as mutants or Neurog3^{ΔAdInt} and Neurog3^{flox/flox} littermates as controls. To induce Neurog3 deletion, 8- to 13-week-old males were treated with tamoxifen (10 mg/30 g body weight mouse) (Sigma-Aldrich) by oral gavage once per day, every second day for 5 days. Mutants and controls were treated with tamoxifen concurrently. Studies were performed with adult males.

Metabolic Studies

Metabolic studies were performed by the Mouse Clinical Institute (MCI) metabolic platform (<http://www.ics-mci.fr>). Body weights were recorded weekly all over the study. At 4 and 10 weeks after the tamoxifen treatment, body composition was determined by magnetic resonance imaging (Minispec+ analyzer, Bruker) and normalized to the weight. At 5 weeks after tamoxifen, food and water consumption as well as stool and urine production were measured over 24 hours in metabolic cages (Tecniplast) after 3 days of acclimatation. The animals were housed individually for 4 days with ad libitum access to food and water. The energy content of stools was evaluated in a bomb calorimeter (C503 control, IKA). The energy excreted was calculated as feces energy content (Cal/g) × feces weight (g). The energy ingested was calculated as food intake per day (g) × diet calorific value (3.34 kcal/g). Food efficiency is the ratio of energy ingested/energy excreted per day.

Blood Analyses

All blood analyses were performed by the MCI metabolic platform (<http://www.ics-mci.fr>). At the end of the metabolic tests, a terminal intracardiac blood sample was taken. Different blood chemistry parameters and a panel of metabolic markers were measured on the plasma samples: total cholesterol, HDL and LDL cholesterol, triglycerides, free fatty acids, glycerol, biliary salts, and lipase.

Short-chain Fatty Acids Measurements

Short-chain fatty acids (acetate, propionate, butyrate, isobutyrate, and valerate) contents were determined in stool samples by gas chromatography-mass spectrometry (GC-MS). Stool samples were weighed (20–50 mg) and dissolved in 200 μL of sodium hydroxide solution at 0.15 M

(Sigma-Aldrich). Short-chain fatty acids dosage was performed as described in Cuffaro et al (PMID: 33803291).⁶⁵

Sterol Measurements

Sterol (cholesterol, desmosterol, lathosterol, campesterol, lanosterol, and sitosterol) contents were determined in stool samples by GC-MS. For quantification, standard solutions of sterols (ranging from 0–500 μg/mL for cholesterol and 0–2 μg/mL for other sterols) were made by serial dilutions of 500 μg/mL and 2 mg/mL (for cholesterol and others sterols, respectively) solution in cyclohexane. Stool samples were weighed (20–50 mg) and diluted 1/10 in distilled water. Sterols were extracted from stool homogenates and standard solutions (100 μL) with 1.5 mL of a cyclohexane and 20 μL of Internal Standards Solution (*D*₇-cholesterol [500 μg/mL] and *D*₆-campesterol [2 μg/mL]). After centrifugation (10 minutes, 4100 rpm, 15 °C), supernatants were dried under a nitrogen stream at 60 °C. Dried samples were dissolved in 500 μL of ethanol 90% and 250 μL of NaOH 1N and heated at 100 °C for 3.5 hours for saponification. Distilled water was added (250 μL), and sterols were extracted with 1.75 mL cyclohexane. After centrifugation (5 minutes, 3000 rpm, 15 °C), supernatants were collected and dried under nitrogen at 60 °C. Dried samples were derivatized with 40 μL of N-methyl-N-trimethylsilyl-trifluoroacetamide (40 minutes, 70 °C, Sigma Aldrich). Samples were evaporated to dryness under a nitrogen stream (60 °C) and reconstituted with cyclohexane (250 μL). GC-MS analyses were performed using 6890 and 5975C inert systems (Agilent Technologies). Sterols and internal standards were eluted on a HP-1MS column (Agilent Technologies, 30 m × 0.25 mm ID × 0.25 μm film) with helium used as gas vector at 1.2 mL/min flow rate. Five microliters were injected into the analytical systems, the injector being set at 250 °C. Separation was achieved using a temperature gradient (70 °C/min from 150 °C to 285 °C, 20 °C/min to 300 °C, 300 °C for 7.5 minutes), and MS ran on electron impact mode for ionization. Single-ion monitoring mode was used at *m/z* ratios of 301, 308, 343, 458, 382, 393, 349, and 396 for cholesterol, *D*₇-cholesterol, desmosterol, lathosterol, campesterol, lanosterol, *D*₆-campesterol, and sitosterol, respectively.

Immuno-histochemistry and Histopathology

Mouse tissues were fixed in paraformaldehyde 4% at 4 °C overnight and processed as previously described.^{12,13} Primary antibodies used for immunostainings: goat anti-ChromograninA (ChrA (C20) sc-1488; Santa Cruz Biotechnology); goat anti-secretin ([S-21] sc-26630; Santa Cruz Biotechnology); rat anti-somatostatin (YC7, MAB354; Chemicon). Secondary antibodies are conjugated to Alexa Fluor 594, DyLight 488, DyLight 549, and DyLight 649 (Jackson ImmunoResearch). Standard histology techniques were performed in collaboration with the MCI (<http://www.ics-mci.fr>).

Morphometric Analyzes

The length of villi (at least 69 units under a CD; at least 20 under an HFD) and colon glands (at least 63 units under a CD) were measured per genotype in well oriented crypt-

villus units using the Fiji software ($n = 3-8$). Evaluation of Oil Red O staining in intestinal epithelium and lamina propria was performed on 2 sections per segment per animal ($n = 5$). Blind scoring was performed according to size and frequency as follows: absence (0), rare very small droplets (0.25), rare small droplets (0.5), frequent small droplets (1), and ubiquitous big droplets (2).

RNA isolation and Reverse Transcriptase-quantitative Polymerase Chain Reaction

The intestine from adult *Neurog3*^{ΔAdInt} and control males was collected 18 weeks (males under CD) and 5 weeks (males under HFD) after tamoxifen administration. Total RNA from duodenum, jejunum, ileum, proximal colon, or distal colon was extracted using NucleoSpin RNA Plus, Mini Kit (Macherey-Nagel) according to the manufacturer's instructions. Reverse transcription was performed using Transcriptor Reverse Transcriptase (Roche) and Random primers (Roche). Quantitative polymerase chain reactions were performed in a Light Cycler 480 (Roche) with Light Cycler 480 Probes Master Mix (Roche) using mouse-specific TaqMan primers and probes (ThermoFisher) recognizing *Neurog3* (Mm00437606_s1), *Cck* (Mm00446170_m1), *Chga* (Mm00514341_m1), *Defa1* (Mm02524428_g1), *Gcg* (Mm00801712_m1), *Ghrl* (Mm00445450_m1), *Gip* (Mm00433601_m1), *mKi67* (Mm01278617_m1), *Lgr5* (Mm00458299_m1), *Lyz1* (Mm00657323_m1), *Muc2* (Mm00458299_m1), *Nts* (Mm00481140_m1), *Olfm4* (Mm01320260_m1), *Pcna* (Mm00448100_g1), *Pyy* (Mm00520715_m1), *Sct* (Mm00441235_g1), *Sst* (Mm00436671_m1), *Tph1* (Mm00493794_m1). Gene expression levels were normalized to *Actb* (4352933E) or *Rplp0* (Mm01974474_gH). Relative changes in gene expression were determined by the $2^{-\Delta\Delta Ct}$ method.

RNA Sequencing and Bioinformatic Analysis

Neurog3^{eYFP/+} mice⁶⁶ (C57BL/6N background), 8 weeks old, were fed with standard CD (Safe D04) or HFD (D12492 Research diet) for 4 weeks. The jejunum was minced and villi enriched by EDTA treatment. Cells were dissociated with dispase and eYFP+ and eYFP- cells sorted (FACS Aria II), RNA was extracted using RNeasy Qiagen columns. Double-stranded cDNAs were prepared from total RNA using Ovation RNA-Seq System V2 (NuGEN Part #7102-32). Libraries were then generated using Ovation SP Ultralow Library Systems (NuGeN, Part #8033) following manufacturer instructions and sequenced on an Illumina HiSeq2500 sequencer (single-end 50bp reads). Reads were mapped onto the mm10 assembly of mouse genome using Tophat v2.0.10⁶⁷ with bowtie v2.1.0.⁶⁸ Gene expression was quantified using HTSeq version 0.5.4p3 and gene annotations from Ensembl release 74. Statistical analysis was performed with R 3.0.1 and DESeq2 1.0.19⁶⁹ Bioconductor library with Benjamini and Hochberg (BH) *P*-value adjustment method.

RNA sequencing was carried out on the duodenum and ileum from adult *Neurog3*^{ΔAdInt} and control males ($n = 4$ /genotype) fed with standard CD or HFD. After tamoxifen administration, samples were collected upon 18 weeks (CD) or 5 weeks (HFD) after. Libraries were prepared using

TruSeq Stranded Total RNA Library Prep Gold kit (Illumina) with either rRNA Removal Mix-Gold (Illumina) or riboPOOL kit (siTOOLs Biotech) at the step of ribodepletion and sequenced on an Illumina HiSeq 4000 or NextSeq 2000 (single-end 50bp reads). Reads were mapped onto the mm39 assembly of mouse genome using STAR⁷⁰ version 2.5.3a. Gene expression was quantified using htseq-count⁷¹ version 0.6.1p1 and gene annotations from Ensembl release 104. Statistical analysis was performed using R 3.3.2 and DESeq2 1.16.1 Bioconductor library and independent hypothesis weighting⁷² *P*-value adjustment method. Gene Ontology enrichment analysis was performed using METASCAPE. Data were deposited in GEO repository (GSE218600, GSE224026, GSE221473).

High Throughput 16S Metagenomic Analysis

Samples and library preparations and preliminary bioinformatic analyses were performed by the MCI (<http://www.ics-mci.fr>). The feces of each mouse were sampled before and 8, 15, 22, and 30 days after tamoxifen administration. DNA was extracted using Nucleospin DNA stool kit (Macherey-Nagel). The region V3-V4 of the 16S rRNA gene was amplified by polymerase chain reaction and paired-end sequenced (2 250bp) using MiSeq Illumina (University of Laval, Canada). Data were deposited at <https://doi.org/10.5281/zenodo.7703798>. FROGS (galaxy-supported pipeline) was used to filter the sets of 16S V3-V4 amplicon sequences described in Escudie et al.⁷³ FROGS was used to produce abundance tables of OTUs and their taxonomic affiliation.⁷³ SILVA was used as reference database for taxonomy affiliation.⁷⁴ Alpha diversity was estimated by the observed OTUs and Shannon index metrics and visualized using R package dplyr v1.0.7, ggplot2 v3.3.5, and ggstatsplot v0.7.2. α -diversity was compared using the Wilcoxon rank-sum test. Beta-diversity ordinations were calculated on the Bray-Curtis dissimilarity matrix using Phyloseq v1.30.0⁷⁵ and ggplot2 packages. Difference between groups was tested using permutational multivariate analysis of variance (PERMANOVA) computed with the Adonis function of the vegan package 2.5.7 with default parameters. Differential abundance analyses were performed at the OTUs level with DESeq2 using Phyloseq v1.30.0 and DESeq2 v1.26.0. The size factor estimation was set to use "poscounts" as suggested for microbiota analysis. Only results displaying an adjusted *P*-value < .05 after BH correction were reported and visualized using ggplot2.

Phylogenetic Investigation of Communities by Reconstruction of Unobserved States (PICRUST2, <https://github.com/picrust/picrust2>; v2.5.1) was used to predict and investigate the metagenome of the bacteria identified using 16S sequences. The analysis was performed using default parameters.⁷⁶ Pathway abundance predictions were computed based on Kyoto Encyclopedia of Genes and Genomes database. ALDEX2 (<https://github.com/ggloor/ALDEX2>)⁷⁷ Cliquez ou appuyez ici pour entrer du texte. statistical analysis was performed to compare pathway abundances of centered-log-ratio (CLR)-transformed data, considering Welch's *t*-test with BH correction. Differentially inferred pathways were visualized in MA plot. Only pathways

with a BH adjusted *P*-value < .05 were considered significant between the 2 conditions and reported in the bar plot.

Statistics

All data are expressed as mean ± standard deviation (SD). Statistical analysis was performed on GraphPad Prism 8.0 or R software with significance set at *P*-value < .05. Longitudinal data and grouped analyzes with 2 factors were analyzed using 2-way analysis of variance (ANOVA) and Holm-Sidak posthoc test. Single comparisons were made with Mann-Whitney tests. The statistical tests and sample sizes are indicated in the figure legends.

References

- Gribble FM, Reimann F. Function and mechanisms of enteroendocrine cells and gut hormones in metabolism. *Nat Rev Endocrinol* 2019;15:226–237.
- Mellitzer G, Gradwohl G. Enteroendocrine cells and lipid absorption. *Curr Opin Lipidol* 2011;22:171–175.
- McCauley HA. Enteroendocrine regulation of nutrient absorption. *J Nutrition* 2019;150:10–21.
- Jenny M, Uhl C, Roche C, et al. Neurogenin3 is differentially required for endocrine cell fate specification in the intestinal and gastric epithelium. *EMBO J* 2002;21:6338–6347.
- Lee CS, Perreault N, Brestelli JE, et al. Neurogenin 3 is essential for the proper specification of gastric enteroendocrine cells and the maintenance of gastric epithelial cell identity. *Gene Dev* 2002;16:1488–1497.
- Spence JR, Mayhew CN, Rankin SA, et al. Directed differentiation of human pluripotent stem cells into intestinal tissue in vitro. *Nature* 2011;470:105–109.
- Egerod KL, Engelstoft MS, Grunddal KV, et al. A major lineage of enteroendocrine cells coexpress CCK, secretin, GIP, GLP-1, PYY, and neurotensin but not somatostatin. *Endocrinology* 2012;153:5782–5795.
- Haber AL, Biton M, Rogel N, et al. A single-cell survey of the small intestinal epithelium. *Nature* 2017;551:333–339.
- Gehart H, van Es JH, Hamer K, et al. Identification of enteroendocrine regulators by real-time single-cell differentiation mapping. *Cell* 2019;176:1158–1173.e16.
- Beumer J, Artegiani B, Post Y, et al. Enteroendocrine cells switch hormone expression along the crypt-to-villus BMP signalling gradient. *Nat Cell Biol* 2018;20:909–916.
- Beumer J, Puschhof J, Bauzá-Martínez J, et al. High-resolution mRNA and secretome atlas of human enteroendocrine cells. *Cell* 2020;181:1291–1306.e19.
- Piccand J, Vagne C, Blot F, et al. Rfx6 promotes the differentiation of peptide-secreting enteroendocrine cells while repressing genetic programs controlling serotonin production. *Mol Metab* 2019;29:24–39.
- Mellitzer G, Beucher A, Lobstein V, et al. Loss of enteroendocrine cells in mice alters lipid absorption and glucose homeostasis and impairs postnatal survival. *J Clin Invest* 2010;120:1708–1721.
- Wang J, Cortina G, Wu SV, et al. Mutant neurogenin-3 in congenital malabsorptive diarrhea. *N Engl J Med* 2006;355:270–280.
- McCauley HA, Matthis AL, Enriquez JR, et al. Enterendocrine cells couple nutrient sensing to nutrient absorption by regulating ion transport. *Nat Commun* 2020;11:4791.
- Lentle RG, Janssen PWM. *The physical processes of digestion*. Macmillan International Higher Education (Springer), 2011.
- Chalhoub G, Kolleritsch S, Maresch LK, et al. Carboxylesterase 2 proteins are efficient diglyceride and monoglyceride lipases possibly implicated in metabolic disease. *J Lipid Res* 2021;62:100075.
- Oteng A-B, Higuchi S, Banks AS, et al. Cyp2c-deficiency depletes muricholic acids and protects against high-fat diet-induced obesity in male mice but promotes liver damage. *Mol Metab* 2021;53:101326.
- Habib SM, Zwicker BL, Wykes L, et al. Sexually dimorphic response of mice to the Western-style diet caused by deficiency of fatty acid binding protein 6 (Fabp6). *Physiological Reports* 2021;9:e14733.
- Quiroga AD, Lian J, Lehner R. Carboxylesterase1/esterase-x regulates chylomicron production in mice. *PLoS One* 2012;7:e49515.
- Abumrad NA, Davidson NO. Role of the gut in lipid homeostasis. *Physiol Rev* 2012;92:1061–1085.
- Anderson GW, Zhu Q, Metkowsky J, et al. The Thrsp null mouse (Thrsptm1cnm) and diet-induced obesity. *Mol Cell Endocrinol* 2009;302:99–107.
- Burchat N, Akal T, Ntambi JM, et al. SCD1 is nutritionally and spatially regulated in the intestine and influences systemic postprandial lipid homeostasis and gut-liver crosstalk. *Biochim Biophys Acta Mol Cell Biol Lipids* 2022;1867:159195.
- Lambert G, Sjouke B, Choque B, et al. The PCSK9 decade Thematic Review Series: new lipid and lipoprotein targets for the treatment of cardiometabolic diseases. *J Lipid Res* 2012;53:2515–2524.
- Su X, Liu S, Zhang X, et al. Requirement of cytosolic phospholipase A2 gamma in lipid droplet formation. *Biochim Biophys Acta Mol Cell Biol Lipids* 2017;1862:692–705.
- Lee JH, Giannikopoulos P, Duncan SA, et al. The transcription factor cyclic AMP-responsive element-binding protein H regulates triglyceride metabolism. *Nat Med* 2011;17:812–815.
- Zhu Y, Gu L, Lin X, et al. USP19 exacerbates lipogenesis and colorectal carcinogenesis by stabilizing ME1. *Cell Reports* 2021;37:110174.
- Iizuka K, Takao K, Yabe D. ChREBP-mediated regulation of lipid metabolism: involvement of the gut microbiota, liver, and adipose tissue. *Front Endocrinol* 2020;11:587189.
- Hu Z, Zhang C, Sifuentes-Dominguez L, et al. Small proline-rich protein 2A is a gut bactericidal protein deployed during helminth infection. *Science* 2021;374:eabe6723.
- Mukherjee S, Hooper LV. Antimicrobial defense of the intestine. *Immunity* 2015;42:28–39.
- Barchetta I, Baroni MG, Melander O, et al. New insights in the control of fat homeostasis: the role of neurotensin. *Int J Mol Sci* 2022;23:2209.

32. Su X, Kong Y, Peng D. New insights into apolipoprotein A5 in controlling lipoprotein metabolism in obesity and the metabolic syndrome patients. *Lipids Health Dis* 2018;17:174.
33. Rader DJ. New therapeutic approaches to the treatment of dyslipidemia. *Cell Metab* 2016;23:405–412.
34. Grabner GF, Zimmermann R, Schicho R, et al. Monoglyceride lipase as a drug target: at the crossroads of arachidonic acid metabolism and endocannabinoid signaling. *Pharmacol Therapeut* 2017;175:35–46.
35. Lawson HA, Zayed M, Wayhart JP, et al. Physiologic and genetic evidence links hemopexin to triglycerides in mice and humans. *Int J Obesity* 2017;41:631–638.
36. Magne F, Gotteland M, Gauthier L, et al. The firmicutes/bacteroidetes ratio: a relevant marker of gut dysbiosis in obese patients? *Nutrients* 2020;12:1474.
37. Sumara G, Sumara O, Kim JK, et al. Gut-derived serotonin is a multifunctional determinant to fasting adaptation. *Cell Metab* 2012;16:588–600.
38. Terry NA, Ngaba LV, Wilkins BJ, et al. Lipid malabsorption from altered hormonal signaling changes early gut microbial responses. *Am J Physiol Gastrointest Liver Physiol* 2018;315:G580–G591.
39. Hilgendorf KI, Johnson CT, Mezger A, et al. Omega-3 fatty acids activate ciliary FFAR4 to control adipogenesis. *Cell* 2019;179:1289–1305.e21.
40. Hussain MM. Intestinal lipid absorption and lipoprotein formation. *Curr Opin Lipidol* 2014;25:200–206.
41. Abdul-Wahed A, Guilmeau S, Postic C. Sweet sixteenth for ChREBP: established roles and future goals. *Cell Metab* 2017;26:324–341.
42. Boer GA, Keenan SN, Miotto PM, et al. GIP receptor deletion in mice confers resistance to high-fat diet-induced obesity via alterations in energy expenditure and adipose tissue lipid metabolism. *Am J Physiol Endocrinol Metab* 2021;320:E835–E845.
43. Benchoula K, Parhar IS, Hwa WE. The molecular mechanism of VGF in appetite, lipids, and insulin regulation. *Pharmacol Res* 2021;172:105855.
44. Bäckhed F, Ding H, Wang T, et al. The gut microbiota as an environmental factor that regulates fat storage. *Proc National Acad Sci U S A* 2004;101:15718–15723.
45. Martinez-Guryn K, Hubert N, Frazier K, et al. Small intestine microbiota regulate host digestive and absorptive adaptive responses to dietary lipids. *Cell Host Microbe* 2018;23:458–469.e5.
46. Fan Y, Pedersen O. Gut microbiota in human metabolic health and disease. *Nat Rev Microbiol* 2021;19:55–71.
47. Psichas A, Sleeth ML, Murphy KG, et al. The short chain fatty acid propionate stimulates GLP-1 and PYY secretion via free fatty acid receptor 2 in rodents. *Int J Obes (Lond)* 2015;39:424–429.
48. Tolhurst G, Heffron H, Lam YS, et al. Short-chain fatty acids stimulate glucagon-like peptide-1 secretion via the G-protein-coupled receptor FFAR2. *Diabetes* 2012;61:364–371.
49. Arora T, Akrami R, Pais R, et al. Microbial regulation of the L cell transcriptome. *Sci Rep* 2018;8:1207.
50. Jawahar J, McCumber AW, Lickwar CR, et al. Starvation causes changes in the intestinal transcriptome and microbiome that are reversed upon refeeding. *BMC Genomics* 2022;23:225.
51. David LA, Maurice CF, Carmody RN, et al. Diet rapidly and reproducibly alters the human gut microbiome. *Nature* 2014;505:559–563.
52. Hildebrandt MA, Hoffmann C, Sherrill-Mix SA, et al. High-fat diet determines the composition of the murine gut microbiome independently of obesity. *Gastroenterology* 2009;137:1716–1724.e2.
53. Turnbaugh PJ, Bäckhed F, Fulton L, et al. Diet-induced obesity is linked to marked but reversible alterations in the mouse distal gut microbiome. *Cell Host Microbe* 2008;3:213–223.
54. Li J, Li X, Song J, et al. Absence of neurotensin attenuates intestinal dysbiosis and inflammation by maintaining Mmp7/ α -defensin axis in diet-induced obese mice. *FASEB J* 2020;34:8596–8610.
55. Li J, Song J, Zaytseva YY, et al. An obligatory role for neurotensin in high-fat-diet-induced obesity. *Nature* 2016;533:411–415.
56. Donaldson GP, Lee SM, Mazmanian SK. Gut biogeography of the bacterial microbiota. *Nat Rev Microbiol* 2016;14:20–32.
57. Hogan SP, Seidu L, Blanchard C, et al. Resistin-like molecule β regulates innate colonic function: Barrier integrity and inflammation susceptibility. *J Allergy Clin Immunol* 2006;118:257–268.
58. Proheteu DC, Chara AL, Harris TA, et al. Resistin-like molecule β is a bactericidal protein that promotes spatial segregation of the microbiota and the colonic epithelium. *Proc National Acad Sci U S A* 2017;114:11027–11033.
59. Shin JH, Bozadjieva-Kramer N, Shao Y, et al. The gut peptide Reg3g links the small intestine microbiome to the regulation of energy balance, glucose levels, and gut function. *Cell Metab* 2022;34:1765–1778.e6.
60. Akahoshi DT, Bevins CL. Flagella at the host-microbe interface: key functions intersect with redundant responses. *Front Immunol* 2022;13:828758.
61. Colin R, Ni B, Laganenka L, et al. Multiple functions of flagellar motility and chemotaxis in bacterial physiology. *FEMS Microbiol Rev* 2021;45:fuab038.
62. Lennicke C, Rahn J, Kipp AP, et al. Individual effects of different selenocompounds on the hepatic proteome and energy metabolism of mice. *Biochim Biophys Acta Gen Subj* 2017;1861:3323–3334.
63. Ku JWK, Gan Y-H. New roles for glutathione: modulators of bacterial virulence and pathogenesis. *Redox Biol* 2021;44:102012.
64. El Marjou FE, Janssen K. Tissue-specific and inducible Cre-mediated recombination in the gut epithelium. *Genesis* 2004;39:186–193.
65. Cuffaro B, Assouhoun ALW, Boutillier D, et al. Identification of New Potential Biotherapeutics from Human Gut Microbiota-Derived Bacteria. *Microorg* 2021;9:565.
66. Mellitzer G, Martín M, Sidhoum-Jenny M, et al. Pancreatic islet progenitor cells in neurogenin 3-yellow fluorescent protein knock-add-on mice. *Mol Endocrinol* 2004;18:2765–2776.
67. Kim D, Perteza G, Trapnell C, et al. TopHat2: accurate alignment of transcriptomes in the presence of insertions, deletions and gene fusions. *Genome Biol* 2013;14:R36.

68. Langmead B, Salzberg SL. Fast gapped-read alignment with Bowtie 2. *Nat Methods* 2012;9:357–359.
69. Love MI, Huber W, Anders S. Moderated estimation of fold change and dispersion for RNA-seq data with DESeq2. *Genome Biol* 2014;15:550.
70. Dobin A, Davis CA, Schlesinger F, et al. STAR: ultrafast universal RNA-seq aligner. *Bioinformatics* 2013;29:15–21.
71. Anders S, Pyl PT, Huber W. HTSeq—a Python framework to work with high-throughput sequencing data. *Bioinformatics* 2015;31:166–169.
72. Ignatiadis N, Klaus B, Zaugg JB, et al. Data-driven hypothesis weighting increases detection power in genome-scale multiple testing. *Nat Methods* 2016;13:577–580.
73. Escudé F, Auer L, Bernard M, et al. FROGS: Find, Rapidly, OTUs with Galaxy Solution. *Bioinformatics* 2017;34:1287–1294.
74. Quast C, Priesse E, Yilmaz P, et al. The SILVA ribosomal RNA gene database project: improved data processing and web-based tools. *Nucleic Acids Res* 2013;41:D590–D596.
75. McMurdie PJ, Holmes S. phyloseq: An R package for reproducible interactive analysis and graphics of microbiome census data. *PLoS One* 2013;8:e61217.
76. Douglas GM, Maffei VJ, Zaneveld JR, et al. PICRUSt2 for prediction of metagenome functions. *Nat Biotechnol* 2020;38:685–688.
77. Fernandes AD, Macklaim JM, Linn TG, et al. ANOVA-Like Differential Expression (ALDEx) Analysis for Mixed Population RNA-Seq. *PLoS One* 2013;8:e67019.

Acknowledgments

The authors thank Guillaume Pavlovic and Loic Lindner, Marie-France Champy and Erwan Grandgirard (Institut Clinique de la Souris) for help in analyzing the microbiota, mice phenotyping and imaging, Cédric Lemay and Filipe de Vadder for helpful discussions, and GG lab members for critical reading of the manuscript. The authors thank IGBMC flow cytometry facility and GenomEast platform for cell sorting and sequencing.

CRedit Authorship Contributions

Florence Blot (Conceptualization: Equal; Formal analysis: Equal; Methodology: Equal; Validation: Equal; Investigation: Equal; Writing – original draft: supporting)

Justine Marchix (Conceptualization: Equal; Data curation: Lead; Formal analysis: Lead; Writing – original draft: Equal; review & editing: Equal)

Miriam Ejarque (Investigation: Equal; Formal analysis: Equal; Methodology: Equal; Validation: Equal)

Sara Jimenez Correa (Formal analysis: Equal; Methodology: Equal; Validation: Equal; Visualization: Equal; Writing – original draft: Supporting)

Aline Meunier (Investigation: Equal; Methodology: Equal; Validation: Equal; Visualization: Equal)

Céline Keime (Data curation: Lead; Formal analysis: Lead; Methodology: Lead; Validation: Lead; Visualization: Supporting; Writing – original draft: Supporting)

Camille Trottier (Data curation: Equal, Formal analysis: Equal)

Mikaël Croyal (Formal analysis: Equal; Methodology: Lead; Validation: Lead; visualization: Equal; Investigation: Supporting; Visualization: Equal)

Maxime M. Mahe (Conceptualization: equal; Funding acquisition: supporting; Methodology: Lead; Supervision: Lead; Writing – original draft: Equal; review & editing: Equal)

Adèle De Arcangelis (Conceptualization: equal; Formal analysis: Equal; Methodology: Equal; Project administration: Equal; Supervision: Equal; Validation: Equal; Visualization: Equal Writing – original draft: Equal; review & editing: Equal)

Gerard Gradwohl, PhD (Conceptualization: Lead; Formal analysis: Lead; Funding acquisition: Lead; Supervision: Lead; Validation: Lead; Writing – original draft: Lead; review & editing: lead)

Conflicts of interest

The authors disclose no conflicts.

Funding

This work was funded by the Novo Nordisk Foundation (Challenge Grant NNF14OC0013655 to Gerard Gradwohl), ANR-21-CE14-0003-01 grant (Gerard Gradwohl and Maxime M. Mahe), ANR Microbiota ANR-19-CE14-0024 grant (Justine Marchix) and Region Pays de Loire (Camille Trottier). Miriam Ejarque was a recipient of a Novo Nordisk Postdoc fellowship. Sequencing was performed by the GenomEast platform, a member of the 'France Génomique' consortium (ANR-10-INBS-0009). IGBMC is supported by the grant ANR-10-LABX-0030-INRT, a French State fund managed by the Agence Nationale de la Recherche under the frame program Investissements d'Avenir ANR-10-IDEX-0002-02.

Received December 4, 2022. Accepted February 16, 2023.

Correspondence

Address correspondence to: Gérard Gradwohl or Adèle De Arcangelis, 1 Rue Laurent Fries, 67404 Illkirch, France. e-mail: adele@igbmc.fr; gradwohl@igbmc.fr; tel: 0033 3 88 65 33 12.